

LPM/99-61
UFR-HEP/99/01
KA-TP-21-1999
February 1999

Associated $H^- W^+$ Production in High Energy e^+e^- Collisions

A. ARHRIB^{1,2}, M. CAPDEQUI PEYRANÈRE³, W. HOLLIK⁴ and G. MOULTAKA³

1: Département de Mathématiques, Faculté des Sciences et Techniques
B.P 416, Tanger, Morocco

2: UFR-High Energy Physics, Physics Department, Faculty of Sciences
PO Box 1014, Rabat-Morocco

3: Laboratoire de Physique Mathématique et Théorique, CNRS-UMR 5825
Université Montpellier II, F-34095 Montpellier Cedex 5, France

4: Institut für Theoretische Physik, Universität Karlsruhe
D-76128 Karlsruhe, Germany

Abstract

We study the associated production of charged Higgs bosons with W gauge bosons in high energy e^+e^- collisions at the one loop level. We present the analytical results and give a detailed discussion for the total cross section predicted in the context of a general Two Higgs Doublet Model (THDM).

1. Introduction

The discovery of the standard Higgs boson is one of the major goals of the present and future searches in particle physics. Direct or indirect results give stringent lower and upper bounds on its mass [1, 2]. Moreover, the problematic scalar sector of the Standard Model (SM) can be enlarged and some simple extensions such as the minimal Two Higgs Doublet Model (THDM) versions [3] are intensively studied. The two most popular versions of the THDM (type I and II), differ in some Higgs couplings to fermions, but in both types and after electroweak symmetry breaking [7], the Higgs spectrum is the same. From the 8 degrees of freedom initially present in the 2 Higgs doublets, 3 correspond to masses of the longitudinal gauge bosons and we are left with 5 degrees of freedom which manifest themselves as 5 physical Higgs particles (2 charged Higgs H^\pm , 2 CP-even H , h and one CP-odd A). The charged Higgs H^\pm , because of its electrical charge, is noticeably different from the other SM or THDM Higgs particles. In other words the discovery of a charged scalar Higgs boson would attest definitively that the Standard Model is overcome. On the contrary a neutral Higgs experimental evidence has to be refined to go beyond the SM[2, 8].

Furthermore, one can construct models with an even larger scalar sector than in the THDM, one of the most popular being the Higgs Triplet Model (HTM) [4]. A noteworthy difference between THDM and HTM is that the HTM contains a tree level $ZW^\pm H^\mp$ coupling while in the THDM this coupling is only generated at one loop level [3, 5]. In models of the HTM type, the physical predictions are sometimes very different from typical ones in the SM and or the THDM. In our study, we will only consider models with two Higgs doublets.

The study of THDM is also very interesting insofar as it provides a general framework to test the minimal supersymmetric extension of the SM (MSSM) [6]. Of course the particle spectrum of the MSSM doubles that of the THDM, but the scalar Higgs sectors, responsible for the electroweak symmetry breaking, are analogous, up to some mass constraints and couplings in the MSSM. In any case, the study of the various production mechanisms of charged Higgs bosons would give information about new physics beyond the SM.

In future colliders or linear accelerators devoted to the electron - positron annihilations, the simplest way to get a charged Higgs is through H^\pm pair production. Such studies have been already undertaken at tree-level [9] and one-loop orders [10, 11] and shown that e^+e^- machines will offer a clean environment and in that sense a higher mass reach, especially if the 1–2 TeV options are available. We mention also that charged Higgs bosons pair production through laser back-scattered $\gamma\gamma$ collisions has been studied in the literature [12] and found to be prominent to discover the charged Higgs boson.

Note also that charged Higgs boson can be produced in hadronic machines:

- (i) single charged Higgs production via $gb \rightarrow tH^-$, $gg \rightarrow t\bar{b}H^-$, $qb \rightarrow q'bH^-$ [13]
- (ii) single charged Higgs production in association with W gauge boson via $gg \rightarrow W^\pm H^\mp$ or $b\bar{b} \rightarrow W^\pm H^\mp$ [14]
- (iii) H^\pm pair production through $q\bar{q}$ annihilation would be feasible only if the charged Higgs decay in top-bottom is kinematically forbidden [15], otherwise one would have to look at bosonic decay modes (ex. $H^\pm \rightarrow h^0 W^\pm$, $H^\pm \rightarrow A^0 W^\pm$, etc...).

The aim of this paper is the study of the production of the charged Higgs boson in association with a W gauge boson through electron positron annihilation. This process is kinematically better suited than the H^\pm pair production when the Higgs mass is larger than the W mass. Although it is a rare process in the THDM, loop or/and threshold effects can give a substantial enhancement. Moreover, once worked out, any experimental deviation from the results within such a model should bring some fruitful information on the new physics.

The paper is organized as follows. In section II, we review all the charged Higgs boson interactions (with gauge bosons, scalar bosons and fermions), section III contains the notations and conventions while section IV is devoted to the on-shell renormalization scheme we will use. In section V we present our numerical results, and section VI contains our conclusions.

2. Charged Higgs boson interactions

2.1 Charged Higgs boson interactions with scalar bosons

In this section we will follow the notation of ref [16]. Recalling the most general (dimension 4) $SU(2)_{weak} \times U(1)_Y$ gauge-invariant and CP-invariant scalar potential for the THDM

$$\begin{aligned} V(\Phi_1, \Phi_2) = & \lambda_1(\Phi_1^+ \Phi_1 - v_1^2)^2 + \lambda_2(\Phi_2^+ \Phi_2 - v_2^2)^2 + \lambda_3((\Phi_1^+ \Phi_1 - v_1^2) + (\Phi_2^+ \Phi_2 - v_2^2))^2 \\ & + \lambda_4((\Phi_1^+ \Phi_1)(\Phi_2^+ \Phi_2) - (\Phi_1^+ \Phi_2)(\Phi_2^+ \Phi_1)) + \lambda_5(Re(\Phi_1^+ \Phi_2) - v_1 v_2)^2 + \\ & \lambda_6[Im(\Phi_1^+ \Phi_2)]^2 + \lambda_7, \end{aligned} \quad (2.1)$$

we have the doublet fields Φ_1 and Φ_2 with weak hypercharge $Y=1$, the corresponding vacuum expectation values v_1 and v_2 , and the coefficients λ_i as real-valued parameters. We will assume the arbitrary additive constant λ_7 to be vanishing. Via the Higgs mechanism, the W and Z gauge bosons acquire masses given by $m_W^2 = \frac{1}{2}g^2 v^2$ and $m_Z^2 = \frac{1}{2}(g^2 + g'^2)v^2$, where g and g' are the $SU(2)_{weak}$ and $U(1)_Y$ gauge couplings and $v^2 = v_1^2 + v_2^2$. The combination $v_1^2 + v_2^2$ is thus fixed by the electroweak scale through $v_1^2 + v_2^2 = (2\sqrt{2}G_F)^{-1}$, and we are left with 7 free parameters in eq.(2.1), namely λ_i and $\tan\beta = v_2/v_1$. As shown in [11], using straight-forward algebra, one can relate the coefficients λ_i of the scalar potential to the masses of the physical Higgs bosons h , H , A , H^\pm [16] in the following way:

$$\lambda_1 = \frac{g^2}{16 \cos^2 \beta m_W^2} [m_H^2 + m_h^2 + (m_H^2 - m_h^2) \frac{\cos(2\alpha + \beta)}{\cos \beta}] + \lambda_3(-1 + \tan^2 \beta) \quad (2.2)$$

$$\lambda_2 = \frac{g^2}{16 \sin^2 \beta m_W^2} [m_H^2 + m_h^2 + (m_h^2 - m_H^2) \frac{\sin(2\alpha + \beta)}{\sin \beta}] + \lambda_3(-1 + \cot^2 \beta) \quad (2.3)$$

$$\lambda_4 = \frac{g^2 m_{H^\pm}^2}{2m_W^2} \quad , \quad \lambda_5 = \frac{g^2}{2m_W^2} \frac{\sin 2\alpha}{\sin 2\beta} (m_H^2 - m_h^2) - 4\lambda_3 \quad , \quad \lambda_6 = \frac{g^2 m_A^2}{2m_W^2} \quad (2.4)$$

Consequently one can choose as free parameters of the Higgs sector: the four Higgs boson masses (m_{H^\pm} , m_H , m_h , m_A), α , $\tan\beta$ and λ_3 .

The trilinear self couplings required for our study are listed in the appendix A, Eqs. (A.1)–(A.7). The trilinear vertices $H^0 H^+ H^-$ and $h^0 H^+ H^-$ depend, besides on the Higgs boson masses, on λ_3 and $\tan\beta$. From Appendix A, eqs.(A.1, A.2), it is obvious that one would get into conflict with the requirements from perturbative unitarity when $\tan\beta$ and/or λ_3 are large. In our analysis we will take into account the following constraints when the masses and the coupling parameters are varied:

- Unitarity constraints will be respected in a simplified way, following [17], by imposing the condition

$$|HHH| < \frac{3g}{2m_W}(1\text{TeV})^2 \quad (2.5)$$

on each trilinear scalar vertex HHH entering the process at one loop.

- Lower bounds on $\tan\beta$ in the general THDM have been obtained from the experimental limits on the processes $e^+e^- \rightarrow Z^* \rightarrow h^0\gamma$ and/or $e^+e^- \rightarrow A^0\gamma$ [18]. For light h masses, these bounds can be rather low [18]. For our study we will restrict the discussion to values $\tan\beta > 0.5$.
- The extra contribution $\delta\rho$ to the ρ parameter [19] should not exceed the current limits from precision measurements [20]:

$$-0.0017 \leq \delta\rho \leq 0.0027$$

2.2 Charged Higgs boson interactions with fermions

In the two-Higgs-doublet extension of the Standard Model there are different ways to couple the Higgs fields to the fermions. Conventionally they are classified in terms of the following categories, labeled as type I and type II models:

- i. **Model type I:** All quarks and leptons couple exclusively to the second Higgs doublet Φ_2 , with the coupling structure copied from the Standard Model. Φ_2 gives mass to both up- and down-type quarks, invoking the charge-conjugate of Φ_2 for the up-type quarks. Since supersymmetry forbids the appearance of the complex conjugate, type I models cannot be realized within the MSSM.
- ii. **Model type II:** To avoid the problem of flavor changing neutral currents (FCNC) [21], one assumes that Φ_1 couples only to down-type quarks and charged leptons and Φ_2 to up-type quarks (and eventually to neutrinos). The type II model is the pattern found in the MSSM.

The general structure of the charged-Higgs boson interaction with a doublet of up- and down-type fermions is given by the vertex

$$[H^- u \bar{d}] = \frac{igV_{ud}}{\sqrt{2}m_W} \left\{ Y_{ud}^L \frac{(1 - \gamma_5)}{2} + Y_{ud}^R \frac{(1 + \gamma_5)}{2} \right\}. \quad (2.6)$$

In the specific models mentioned above, the Yukawa couplings have the form

$$\begin{aligned} Y_{ud}^L &= \frac{m_u}{\tan \beta} & \text{and} & \quad Y_{ud}^R = -\frac{m_d}{\tan \beta} & \text{for model I,} \\ Y_{ud}^L &= \frac{m_u}{\tan \beta} & \text{and} & \quad Y_{ud}^R = m_d \tan \beta & \text{for model II.} \end{aligned} \quad (2.7)$$

V_{ud} is the CKM matrix element, which we will approximate by unity. Models I and II lead to similar results as far as the effects originating from the top–bottom loops for $\tan \beta$ close to 1 are considered, owing essentially to the form of the Yukawa couplings Y^R and Y^L .

2.3 Charged Higgs-boson interactions with gauge bosons

The interactions between the charged Higgs bosons of a two-doublet model and the gauge bosons are completely dictated by local gauge invariance and thus independent of the assumption whether the model is supersymmetric or not. These interactions follow from the kinetic term, involving the covariant derivative, in the Higgs Lagrangian

$$\begin{aligned} \sum_i (D_\mu \Phi_i)^+ (D_\mu \Phi_i) = & \\ \sum_i [(\partial_\mu + ig \vec{T}_a \vec{W}_\mu^a + ig' \frac{Y_{\Phi_i}}{2} B_\mu) \Phi_i]^+ [(\partial_\mu + ig \vec{T}_a \vec{W}_\mu^a + ig' \frac{Y_{\Phi_i}}{2} B_\mu) \Phi_i], & \end{aligned} \quad (2.8)$$

where \vec{T}_a is the isospin operator and Y_{Φ_i} the hypercharge of the Higgs fields; W_μ^a denote the $SU(2)_L$ gauge fields, B_μ the $U(1)_Y$ gauge field, and g (resp. g') the associated coupling constants. The individual couplings in the various vertices, derived from eq. (2.8), are listed in Appendix C. The $\gamma H^\mp W^\pm$ and the $Z H^\mp W^\pm$ vertices vanish at the tree level. Therefore, tree-level contributions to $e^+ e^- \rightarrow W^\pm H^\mp$ come only from neutrino exchange in the t -channel and from CP-even Higgs mediated s-channel. All these contributions are strongly suppressed by the small electron mass. Hence, the process under study is essentially a loop-mediated process.

3. Notations and conventions

We will use the following notations and conventions. The momenta of the incoming electron and positron, outgoing gauge boson W^+ and outgoing Higgs boson H^- are denoted by p_1 , p_2 , k_1 and k_2 , respectively. Neglecting the electron mass, the momenta, in the $e^+ e^-$ center-of-mass system, are given by:

$$\begin{aligned} p_{1,2} &= \frac{\sqrt{s}}{2} (1, 0, 0, \pm 1) \\ k_{1,2} &= \frac{\sqrt{s}}{2} \left(1 \pm \frac{m_W^2 - m_{H^\pm}^2}{s}, \pm \kappa \sin \theta, 0, \pm \kappa \cos \theta \right), \end{aligned}$$

where \sqrt{s} denotes the center of mass energy, θ the scattering angle between e^- and W^+ , and κ is determined by

$$\kappa^2 = (s - (m_{H^\pm} + m_W)^2)(s - (m_{H^\pm} - m_W)^2)/s^2.$$

The Mandelstam variables are defined as follows:

$$\begin{aligned} s &= (p_1 + p_2)^2 = (k_1 + k_2)^2 \\ t &= (p_1 - k_1)^2 = (p_2 - k_2)^2 = \frac{1}{2}(m_W^2 + m_{H^\pm}^2) - \frac{s}{2} + \frac{s}{2}\kappa \cos \theta \\ u &= (p_1 - k_2)^2 = (p_2 - k_1)^2 = \frac{1}{2}(m_W^2 + m_{H^\pm}^2) - \frac{s}{2} - \frac{s}{2}\kappa \cos \theta \\ s + t + u &= m_W^2 + m_{H^\pm}^2. \end{aligned}$$

The differential cross section reads, expressed in terms of the one-loop amplitude \mathcal{M}^1 :

$$\frac{d\sigma}{d\Omega}(e^+e^- \rightarrow W^\pm H^\mp) = \frac{\kappa}{64\pi^2 s} \sum_{Pol} |\mathcal{M}^1|^2. \quad (3.1)$$

\mathcal{M}^1 can be decomposed into six invariant matrix elements \mathcal{A}_i and scalar coefficient functions \mathcal{M}_i as follows:

$$\mathcal{M}^1 = \sum_{i=1}^6 \mathcal{M}_i \mathcal{A}_i. \quad (3.2)$$

The basic matrix elements \mathcal{A}_i are given by the following expressions:

$$\begin{aligned} \mathcal{A}_1 &= \bar{v}(p_2) \not{\epsilon}(k_1) \frac{1 + \gamma_5}{2} u(p_1) \\ \mathcal{A}_2 &= \bar{v}(p_2) \not{\epsilon}(k_1) \frac{1 - \gamma_5}{2} u(p_1) \\ \mathcal{A}_3 &= \bar{v}(p_2) \not{k}_1 \frac{1 + \gamma_5}{2} u(p_1) (p_1 \cdot \epsilon(k_1)) \\ \mathcal{A}_4 &= \bar{v}(p_2) \not{k}_1 \frac{1 - \gamma_5}{2} u(p_1) (p_1 \cdot \epsilon(k_1)) \\ \mathcal{A}_5 &= \bar{v}(p_2) \not{k}_1 \frac{1 + \gamma_5}{2} u(p_1) (p_2 \cdot \epsilon(k_1)) \\ \mathcal{A}_6 &= \bar{v}(p_2) \not{k}_1 \frac{1 - \gamma_5}{2} u(p_1) (p_2 \cdot \epsilon(k_1)). \end{aligned} \quad (3.3)$$

The squared amplitude, after summation over the polarizations of the W^+ boson, gets the following form:

$$\begin{aligned} \sum_{Pol} |\mathcal{M}^1|^2 &= 2s(|\mathcal{M}_1|^2 + |\mathcal{M}_2|^2) - \frac{(m_{H^\pm}^2 m_W^2 - tu)}{4m_W^2} \{4|\mathcal{M}_1|^2 + 4|\mathcal{M}_2|^2 \\ &+ 4(m_W^2 - t)Re[\mathcal{M}_1 \mathcal{M}_3^* + \mathcal{M}_2 \mathcal{M}_4^*] + (m_W^2 - t)^2 [|\mathcal{M}_3|^2 + |\mathcal{M}_4|^2] \\ &+ 4(m_W^2 - u)Re[\mathcal{M}_1 \mathcal{M}_5^* + \mathcal{M}_2 \mathcal{M}_6^*] + (m_W^2 - u)^2 [|\mathcal{M}_5|^2 + |\mathcal{M}_6|^2] \\ &- 2(m_{H^\pm}^2 m_W^2 + m_W^2 s - tu)Re[\mathcal{M}_3 \mathcal{M}_5^* + \mathcal{M}_4 \mathcal{M}_6^*]\} \end{aligned} \quad (3.4)$$

The coefficient functions \mathcal{M}_i can be read off from the explicit expressions in Appendix C, according to the decomposition (3.2).

4. On-shell renormalization

We have evaluated the one-loop induced process $e^+e^- \rightarrow W^\pm H^\mp$ in the 't Hooft - Feynman gauge, and using dimensional regularization [22]. The types of Feynman diagrams are depicted in Figure 1. It displays the corrections to the γ - $W^\pm H^\mp$ and to the Z - $W^\pm H^\mp$ vertices, box diagrams, contributions coming from the various mixings H^-W^+ and H^-G^+ in t and s channels, and finally the counter-terms. Note that the s -channel H^-W^+ mixing (Fig. 1.16) vanishes for an on-shell transverse W gauge boson. There is no contribution from the W^+G^- mixing because the γ - $G^\pm H^\mp$ and Z - $G^\pm H^\mp$ vertices are absent at the tree level. All the Feynman diagrams have been generated and computed using FeynArts [23] and FeynCalc [24] packages. We also use the fortran FF-package [25] in the numerical analysis.

Although the amplitude for our process vanishes at the tree level, complications like tadpole contributions and vector boson-scalar mixings require a careful treatment of renormalization. We adopt the on-shell renormalization scheme of [26], for the Higgs sector, which is an extension of the on-shell scheme in [27]. In this scheme, field renormalization is performed in the manifest-symmetric version of the Lagrangian. A field renormalization constant $Z_{\Phi_{1,2}}$ is assigned to each Higgs doublet $\Phi_{1,2}$. The Higgs fields and vacuum expectation values v_i are renormalized as follows:

$$\begin{aligned}\Phi_i &\rightarrow (Z_{\Phi_i})^{1/2}\Phi_i \\ v_i &\rightarrow (Z_{\Phi_i})^{1/2}(v_i - \delta v_i).\end{aligned}\quad (4.1)$$

With these substitutions in the Lagrangian (2.8), expanding the renormalization constants $Z_i = 1 + \delta Z_i$ to the one-loop order, we obtain all the counter-terms relevant for our process: a counter-term for the $W - H$ 2-point function, and counter-terms for the γWH and ZWH vertices, visualized in Fig.1.26 to Fig.1.28 (k_1 denotes the momentum of the outgoing W^+),

$$\delta[W_\nu^\pm H^\mp] = -k_1^\mu \Delta \quad (4.2)$$

$$\delta[A_\nu W_\mu^\pm H^\mp] = ieg_{\mu\nu} \Delta \quad (4.3)$$

$$\delta[Z_\nu W_\mu^\pm H^\mp] = ieg_{\mu\nu} \frac{s_W}{c_W} \Delta \quad (4.4)$$

with

$$\Delta = \frac{\sin 2\beta}{2} m_W \left[\frac{\delta v_1}{v_1} - \frac{\delta v_2}{v_2} + \frac{1}{2} (\delta Z_{\Phi_2} - \delta Z_{\Phi_1}) \right]. \quad (4.5)$$

In the on-shell scheme, the following renormalization conditions are imposed:

- The renormalized tadpoles, i.e. the sum of tadpole diagrams $T_{h,H}$ and tadpole counter-terms $\delta_{h,H}$ vanish:

$$T_h + \delta t_h = 0, \quad T_H + \delta t_H = 0.$$

These conditions guarantee that $v_{1,2}$ appearing in the renormalized Lagrangian $\mathcal{L}_{\mathcal{R}}$ are located at the minimum of the one-loop potential.

- The real part of the renormalized non-diagonal self-energy $\hat{\Sigma}_{H-W^+}(k^2)$ vanishes for an on-shell charged Higgs boson:

$$Re\hat{\Sigma}_{H-W^+}(m_{H^\pm}^2) = 0 \quad (4.6)$$

(the $\hat{\cdot}$ labels the renormalized quantity which is given in Appendix C). This renormalization condition determines the term Δ , and consequently $\delta[A_\nu W_\mu^\pm H^\mp]$ and $\delta[Z_\nu W_\mu^\pm H^\mp]$ are also fixed. The explicit expressions are given in Appendix C.

The last renormalization condition is sufficient to discard the real part of the $H^+ - G^+$ mixing contribution as well. Indeed, using the Slavnov–Taylor identity [28], [29]

$$k^2 \Sigma_{H-W^+}(k^2) - m_W \Sigma_{H-G^+}(k^2) = 0 \quad \text{at} \quad k^2 = m_{H^\pm}^2$$

valid also for the renormalized quantities, together with eq. (4.6), it follows that

$$Re\hat{\Sigma}_{H-G^+}(m_{H^\pm}^2) = 0.$$

In particular, the Feynman diagrams depicted in Fig. 1.25 will not contribute with the above renormalization conditions, being purely real valued.

The amplitudes corresponding to the two counter-terms (photon and Z boson exchanges) in eqs. (4.3, 4.4) contain only the matrix elements \mathcal{A}_1 and \mathcal{A}_2 as follows:

$$\begin{aligned} \mathcal{M}_{CT}^\gamma &= -\frac{e^2}{s} \Delta(\mathcal{A}_1 + \mathcal{A}_2) \\ \mathcal{M}_{CT}^\gamma &= -\frac{e^2}{s - m_Z^2} \frac{s_W}{c_W} \Delta((g_A + g_V)\mathcal{A}_2 + (g_V - g_A)\mathcal{A}_1) \end{aligned} \quad (4.7)$$

with the electron–Z coupling constants

$$g_V = \frac{1}{4s_W c_W} (1 - 4s_W^2), \quad g_A = \frac{1}{4s_W c_W} \quad (4.8)$$

and $s_W \equiv \sin \theta_W$, $c_W \equiv \cos \theta_W$. As a consequence, only the form factors \mathcal{M}_1 and \mathcal{M}_2 can contain UV divergences; each of the remaining form factors should be UV finite by itself, which provides a good analytical check of the calculations.

5. Numerical results and discussion

The difference between the predicted cross sections in Model-I and Model-II is essentially due to the fermion loops containing the different Yukawa couplings. For small values of $\tan \beta$ the cross sections are approximately the same for both models of type I and II (Figure

2a). For $\tan \beta > 10$ (Figure 2b), the cross section decreases to very small values in Model-I, corresponding to the Yukawa coupling proportional to $1/\tan \beta$. In Model-II, the cross section has a minimum for $\tan \beta \approx 30$ and increases again for large $\tan \beta$, following the b Yukawa coupling proportional to $\tan \beta$.

In the following more explicit discussion we consider the range $0.5 \leq \tan \beta < 10$, where both type I and II models give practically the same numerical results. In this interval for $\tan \beta$ the total cross section varies from 7.5 fb to 0.012 fb , for $\sqrt{s} = 500 \text{ GeV}$ and $m_{H^\pm} = 220 \text{ GeV}$.

We will take the following experimental input for the physical parameters [30]:

- the fine structure constant: $\alpha = \frac{e^2}{4\pi} = 1/137.03598$.
- the gauge boson masses: $M_Z = 91.187 \text{ GeV}$ and $M_W = 80.41 \text{ GeV}$. In the on-shell scheme we define $\sin^2 \theta_W$ by $\sin^2 \theta_W \equiv 1 - \frac{M_W^2}{M_Z^2}$, so that it receives by definition no loop corrections.
- the top and bottom quarks masses are taken to be: $m_t = 175 \text{ GeV}$ and $m_b = 4.5 \text{ GeV}$.

Fig.3 shows the top-bottom contribution to the integrated cross section as a function of the center of mass energy \sqrt{s} for four values of m_{H^\pm} and for two values of $\tan \beta$, 0.6 and 1.6. It can be seen that for a small $\tan \beta$ (Fig.3.a) the top quark effect is enhanced. One can reach a cross section of 3.5 fb for a charged Higgs mass of about 220 GeV. The cross section is enhanced for $m_{H^\pm} = 170 \text{ GeV}$ owing to the proximity of the normal threshold cut of the three-point function at $m_{H^\pm} = m_t + m_b$.

As $\tan \beta$ increases the top quark effect decreases, leading to almost an order of magnitude suppression of the cross section for $\tan \beta = 1.6$ (Fig. 3.b). For large values of $\tan \beta (\simeq 50)$ the bottom quark contribution becomes leading and of comparable magnitude to that of the top quark in the small $\tan \beta$ region.

For the general THDM we will present our numerical results in the following three configurations (where all the masses are in GeV):

- C_1 : $m_{H^\pm} = 220$, $m_H = 180$, $m_h = 90$, $m_A = 80$, $\tan \alpha = 1.4$, $\tan \beta = 3.6$
- C_2 : $m_{H^\pm} = 300$, $m_H = 280$, $m_h = 120$, $m_A = 220$, $\tan \alpha = 2.4$, $\tan \beta = 1.6$
- C_3 : $m_{H^\pm} = 400$, $m_H = 380$, $m_h = 120$, $m_A = 370$, $\tan \alpha = 3$, $\tan \beta = 2$

In those three cases the present experimental bound on $\delta\rho$ is respected. In Fig.4.a,b,c we show the total cross section (including all virtual boson and fermion contributions) as a function of the center of mass energy \sqrt{s} for the three configurations listed above and for four different values of λ_3 which satisfy the nominal unitarity constraints (2.5) One can see from those curves that, for a fixed $\tan \beta$, the cross section increases with λ_3 . The effect of λ_3 arises essentially via the trilinear vertices $H^0 H^+ H^-$ and $h^0 H^+ H^-$. Note that values of λ_3 larger than the ones chosen in Fig.4.a,b,c start violating the unitarity constraints on the $H^0 H^+ H^-$ and $h^0 H^+ H^-$ couplings.

Fig.4.d shows the (λ_3 independent) box contributions to the cross section in the $C_{1,2,3}$ configurations. This contribution remains generically suppressed (0.01–0.005 fb for $\sqrt{s} = 500$ –1000 GeV), even in the favourable light Higgs mass configurations such as in case C_1 .

Figures 5.a, 5.b and 5.c show the total cross section as a function of $\tan\beta$ in the $C_{1,2,3}$ configurations with $\lambda_3 = 0.1$, and for $\sqrt{s} = 500$ GeV, 1 TeV and 1.5 TeV respectively. One can see that the cross section reaches a minimum for moderate values of $\tan\beta$ while it gets much larger (a few orders of magnitude) for both low and high values of this parameter. The first enhancement (small $\tan\beta$) is due to the top quark effect as discussed above, while the second enhancement comes from the effect of large $\tan\beta$ in $H^0 H^+ H^-$ and $h^0 H^+ H^-$ couplings. With the parameter choice of Fig.5, the nominal unitarity condition (2.5) forbids $\tan\beta$ larger than 14. One should, however, stress that a different choice of the Higgs masses and λ_3 closer to the MSSM configurations would suppress the Higgs sector effect in the large $\tan\beta$ regime, thus allowing even larger $\tan\beta$ values to be consistent with Eq.(2.5). In this case large effects from the bottom quark sector become dominant.

In Fig.6 we show the dependence of the cross section on the charged Higgs mass for $\sqrt{s} = 500$ GeV, 1 TeV and 1.5 TeV in the case where $\tan\beta = 2$, $\tan\alpha = 3$, $\lambda_3 = 0.1$, $m_H = 180$ GeV, $m_h = 90$ and $m_A = 80$ GeV. One notes the high sensitivity of the cross section to the Higgs mass when the latter is above the $W^- h$ and $b\bar{t}$ decay thresholds (which happen to roughly coincide owing to our input values, and correspond to the kink in the plots). Below this threshold, the cross-section is much less sensitive to the Higgs mass, however, one should keep in mind that this region corresponds to the opening of the charged Higgs pair production which yields a much more interesting event rate.

Finally we mention that our results are in qualitative agreement with those of ref.[32], inasmuch as we can compare. Note however that we did not assume any Higgs mass rules, and also the renormalization scheme in [32] was not explicitly defined.

5. Conclusion

To summarize, we have computed the associate production of charged Higgs boson with a gauge boson W at high energy e^+e^- collisions. The calculation is performed within the dimensional regularisation in the on shell scheme. The study is done in the general two Higgs doublet model taking into account constraints on the ρ parameter and unitarity constraints on the trilinear Higgs couplings. We have shown that in the small $\tan\beta$ regime the top effect is enhanced leading to important cross sections (about 1 fb), while the leading contributions in the large $\tan\beta$ regime, come from the trilinear $HH^\pm H^\mp$ and $hH^\pm H^\mp$ vertices. If the charged Higgs is too heavy to be produced in pairs in e^+e^- future machines, the associate production with a W boson would be the only means to look for direct evidence for it. The smallness of the cross section would require, however, a very high luminosity option.

References

- [1] ALEPH Collaboration, Phys.Lett. **B440** (1998) 403.
- [2] G. Abbiendi et al, OPAL Collaboration, CERN-EP/98-173 hep-ex/9811025.
- [3] J.F. Gunion, H.E. Haber, G.L. Kane and S. Dawson, *The Higgs Hunter's Guide* (Addison-Wesley, Reading, 1990).
- [4] R.N. Mohapatra and J. Pati, Phys. Rev. **D11** (1975) 566.
- [5] M.C. Peyranère, H.E. Haber and P. Irulegui, Phys.Rev. **D44** (1991) 191.
- [6] For reviews see: H.P. Nilles, Phys. Rep. 110 (1984) 1;
H.E. Haber and G.L. Kane, Phys. Rep. 117 (1985) 75.
- [7] H. Komatsu and J. Kubo, Phys. Lett. **B157** (1985) 90; Nucl. Phys. **B263** (1986) 265.
- [8] K. Ackerstaff et al, OPAL Collaboration Eur.Phys.J. **C5** (1998) 19;
M. Carena, S. Mrenna and C. E. M. Wagner, CERN-TH/98-262, hep-ph/9808312.
- [9] S. Komamiya, Phys. Rev. **D38** (1988) 2158; A.Brignole et al.in Proceedings of the Workshop on e^+e^- Collisions at 50 GeV The Physics Potential, ed. P.M.Zerwas, DESY 92-123; A.Djouadi, J.Kalinowski, P.M.Zerwas, *ibid* and Z.Phys.C57 (1993) 569.
- [10] A. Arhrib, M. Capdequi Peyranère and G. Moultaka, Phys. Lett. **B341** (1995) 313;
Marco A. Diaz and Tonnis A. ter Veldhuis hep-ph/9501315, DPF94 Proceedings; J. Guasch, W. Hollik and A. Kraft KA-TP-19-1999, hep-ph/9911452.
- [11] A. Arhrib, and G. Moultaka, Nucl. Phys. **B558** (1999) 3, hep-ph/9808317.
- [12] D. Bowser-Chao et al, Phys. Lett. **B315** (1995) 313; W. G. Ma et al Phys. Rev. **D53** (1996) 1304 and Shou Hua Zhu, Chong Sheng Li and Chong Shou Gao hep-ph/9712367.
- [13] V. Barger, R.J.N. Phillips and D. P. Roy, Lett. **B324**, (1994) 236;
J. F. Gunion, H. E. Haber, F. E. Paige, W. K. Tung and S. S. D. Willenbrock, Nucl. Phys. **B294** (1987) 621; R. M Barnet, H. E. Haber and D. E. Soper, Nucl. Phys. B306, (1988) 697; F. I. Olness and W. K. Tung, Nucl. Phys. **B308**, (1988) 813;
J. L. Diaz-Cruz and O. A. Sampayo, Phys. Rev. **D50**, (1994) 6820;
S. Moretti and K. Odagiri, Phys. Rev. **D55** (1997) 5627.
- [14] D. A. Dicus, J. L. Hewett, C. Kao and T. G. Rizzo, Phys. Rev. **D40** (1989) 787;
A. A. Barrientos Bendezú and B. A. Kniehl, Phys.Rev.D59 (1999) 015009, hep-ph/9807480.

- [15] V. Barger and R.J.N. Phillips, Phys. Rev. **D41**, (1990) 884; A. C. Bawa, C.S. Kim and A. D. Martin, Z. Phys. **C47** (1990) 75; R.M. Godbole and D.P. Roy Phys. Rev. **D43** (1991) 3640; M. Drees and D.P. Roy Phys. Lett. **B269** (1991) 155.
- [16] J. F. Gunion and H. E. Haber, Nucl.Phys. **B272** (1986) 1 and Errata hep-ph/9301205.
- [17] R. Casalbuoni, D. Dominici, F. Feruglio, R. Gatto Nucl. Phys. **B299** (1988) 117.
- [18] M. Krawczyk, hep-ph/9803484, Presented at Workshop on Physics at the First Muon Collider and at the Front End of the Muon Collider, Batavia, IL, 6-9 Nov 1997. see also hep-ph/9812536
M. Krawczyk, J. Zochowski and P. Mattig, DESY-98-177, hep-ph/9811256.
- [19] A. Denner, R.J. Guth, W. Hollik and J.H. Kühn, Z. Phys. **C51** (1991) 695.
- [20] J. Erler and P. Langacker, talk given at the 5th International Wein Symposium (WEIN 98), Santa Fe, Jun 1998, hep-ph/9809352.
- [21] S. Glashow and S. Weinberg, Phys.Rev. **D15** (1977) 1958.
- [22] G. 't Hooft and M. Veltman, Nucl. Phys. **B44** (1972) 189;
P. Breitenlohner and D. Maison, Commun. Math. Phys. **52** (1977) 11.
- [23] H.Eck and J. Kublbeck, Guide to FeynArts 1.0, University of Wurzburg, 1992.
- [24] R.Mertig, Guide to FeynCalc 1.0, University of Wurzburg, 1992.
- [25] G.J. van Oldenborgh, Comput.Phys.Commun. **66** (1991) 1.
- [26] A. Dabelstein, Z. Phys. **C 67** (1995) 495.
- [27] M.Böhm, W.Hollik and H.Spiesberger, Fortschr. Phys. **34** (1986) 11.
- [28] J.A Coarasa, D.Garcia, J.Guasch, R.A.Jimenez and J.Sola, Eur.Phys.J. **C2** (1998) 373.
- [29] M. Capdequi Peyranère, Int. J. Mod. Phys. A14 (1999) 429, hep-ph/9809324.
- [30] C. Caso et al, The European Physical Journal **C3** (1998) 1.
- [31] G. Passarino and M. Veltman, Nucl. Phys. **B160** (1979) 151;
G. 'tHooft and M. Veltman, Nucl. Phys. **B153** (1979) 365.
- [32] S.H. Zhu hep-ph/9901221.

Figure Captions:

Fig. 1: Feynman diagrams relevant for the $e^+e^- \rightarrow W^+H^-$. Fig.1.1 → Fig.1.11 vertex diagrams, Fig.1.12 box diagram, Fig.1.13 → Fig.1.16 typical diagrams contributing the self energies mixing of W^+H^- and G^+H^- , self-energies of the mixing W^+H^- Fig.1.17 → Fig.1.20, self-energies of the mixing G^+H^- Fig.1.21 → Fig.1.25. Fig.1.26 and Fig.1.27 are the counter term for the mixing G^+H^- and W^+H^- . Fig. 1.28 are the counter-terms for the photon- W^+H^- and Z- W^+H^- vertices.

Fig. 2: Top-bottom contribution to the integrated cross section as a function of $\tan\beta$ in Model type I and II for $m_{H^\pm} = 220\text{GeV}$, and $\sqrt{s} = 500\text{GeV}$.

Fig. 3: Top-bottom contribution to the integrated cross section as a function of \sqrt{s} for four values of $m_{H^\pm} = 140\text{GeV}$, 185GeV , 300GeV , and 400GeV . Fig. 3.a $\tan\beta = 0.6$ and Fig. 3.b $\tan\beta = 1.6$

Fig. 4: Integrated total cross section as a function of \sqrt{s} for four values of λ_3 .

Fig. 4.a C_1 case: $m_{H^\pm} = 220$, $m_H = 180$, $m_h = 90$, $m_A = 80$, $\tan\alpha = 1.4$, $\tan\beta = 3.6$

Fig. 4.b C_2 case: $m_{H^\pm} = 300$, $m_H = 280$, $m_h = 120$, $m_A = 220$, $\tan\alpha = 2.4$, $\tan\beta = 1.6$

Fig. 4.c C_3 case: $m_{H^\pm} = 400$, $m_H = 380$, $m_h = 120$, $m_A = 370$, $\tan\alpha = 3$, $\tan\beta = 2$ (where all masses are in GeV)

Fig. 4.d Box contributions to the total cross section as function of the center of mass energy for $C_{1,2,3}$ configurations.

Fig. 5: Integrated total cross section as a function of $\tan\beta$ in the case of the $C_{1,2,3}$ configurations with $\lambda_3 = 0.1$ and for $\sqrt{s} = 500$ GeV (Fig5.a), 1 TeV (Fig.5.b) and 1.5 TeV (Fig.5.c) respectively.

Fig. 6: Integrated total cross section as a function of m_{H^\pm} for $\sqrt{s} = 500$, 1000, and 1500 GeV, with $\tan\beta = 2$, $\tan\alpha = 3$, $\lambda_3 = 0.1$, $m_H = 180$ GeV, $m_h = 90$ GeV and $m_A = 80$ GeV

Appendix A:

In this section we list the Feynman rules for the 3-point vertices involving charged Higgs bosons, in the general THDM.

$$\begin{aligned} g_{H^0 H^+ H^-} &= -i \frac{g}{m_W} [\cos(\beta - \alpha) (m_{H^\pm}^2 - \frac{m_H^2}{2}) + \frac{\sin(\alpha + \beta)}{\sin 2\beta} \{4\lambda_3 v^2 + \frac{1}{2}(m_H^2 + m_h^2) \\ &\quad - \frac{1}{2 \sin 2\beta} (\sin 2\alpha + 2 \sin(\alpha - \beta) \cos(\alpha + \beta)) (m_H^2 - m_h^2)\}] \end{aligned} \quad (\text{A.1})$$

$$\begin{aligned} g_{h^0 H^+ H^-} &= -i \frac{g}{m_W} [\sin(\beta - \alpha) (m_{H^\pm}^2 - \frac{m_h^2}{2}) + \frac{\cos(\alpha + \beta)}{\sin 2\beta} \{4\lambda_3 v^2 + \frac{1}{2}(m_H^2 + m_h^2) \\ &\quad - \frac{1}{2 \sin 2\beta} (\sin 2\alpha + 2 \sin(\alpha + \beta) \cos(\alpha - \beta)) (m_H^2 - m_h^2)\}] \end{aligned} \quad (\text{A.2})$$

$$g_{H^0 H^\pm G^\mp} = \frac{-ig \sin(\beta - \alpha) (m_{H^\pm}^2 - m_H^2)}{2m_W} \quad (\text{A.3})$$

$$g_{h^0 H^\pm G^\mp} = \frac{ig \cos(\beta - \alpha) (m_{H^\pm}^2 - m_h^2)}{2m_W} \quad (\text{A.4})$$

$$g_{A^0 H^\pm G^\mp} = \mp \frac{m_{H^\pm}^2 - m_A^2}{v\sqrt{2}} \quad (\text{A.5})$$

$$g_{H^0 G^+ G^-} = -im_H^2 \frac{\cos(\beta - \alpha)}{\sqrt{2}v} \quad (\text{A.6})$$

$$g_{h^0 G^+ G^-} = -im_h^2 \frac{\sin(\beta - \alpha)}{\sqrt{2}v} \quad (\text{A.7})$$

The parameter λ_3 enters only $g_{H^0 H^+ H^-}$ and $g_{h^0 H^+ H^-}$, while the vertices $g_{H^0 H^\pm G^\mp}$, $g_{h^0 H^\pm G^\mp}$ and $g_{A^0 H^\pm G^\mp}$ have a particularly simple form, proportional to m_H^2 and m_h^2 , respectively.

Appendix B: One-loop functions

Let us briefly recall the definitions of scalar and tensor integrals [31] we use. The inverse of the propagators are denoted by

$$d_0 = q^2 - m_0^2, \quad d_i = (q + p_i)^2 - m_i^2$$

where the p_i are the momenta of the external particles (always incoming).

One-point function:

$$A_0(m_0^2) = \frac{(2\pi\mu)^{(4-D)}}{i\pi^2} \int d^D q \frac{1}{d_0}$$

where μ is an arbitrary renormalization scale and D is the space-time dimension.

Two-point functions:

(the arguments for the tensor integrals on the l.h.s. are incorrect because they depend also on the momenta themselves, not only on their squares)

$$B_{0,\mu} = \frac{(2\pi\mu)^{(4-D)}}{i\pi^2} \int d^D q \frac{\{1, q_\mu\}}{d_0 d_1}$$

Using Lorentz covariance, one gets for the vector integral

$$B_\mu = p_{1\mu} B_1$$

with the scalar function $B_1(p_1^2, m_0^2, m_1^2)$.

Three-point functions:

$$C_{0,\mu,\mu\nu} = \frac{(2\pi\mu)^{(4-D)}}{i\pi^2} \int d^D q \frac{\{1, q_\mu, q_\mu q_\nu\}}{d_0 d_1 d_2}$$

where $p_{ij}^2 = (p_i + p_j)^2$. Lorentz covariance yields the decomposition

$$C_\mu = p_{1\mu} C_1 + p_{2\mu} C_2 \quad (\text{B.1})$$

$$C_{\mu\nu} = g_{\mu\nu} C_{00} + p_{1\mu} p_{1\nu} C_{11} + p_{2\mu} p_{2\nu} C_{22} + (p_{1\mu} p_{2\nu} + p_{2\mu} p_{1\nu}) C_{12} \quad (\text{B.2})$$

with the scalar functions $C_{i,ij}(p_1^2, p_{12}^2, p_2^2, m_0^2, m_1^2, m_2^2)$.

Four-point functions:

$$D_{0,\mu,\mu\nu} = \frac{(2\pi\mu)^{(4-D)}}{i\pi^2} \int d^D q \frac{\{1, q_\mu, q_\mu q_\nu\}}{d_0 d_1 d_2 d_3} \quad (\text{B.3})$$

Again, Lorentz covariance allows the decomposition

$$D_\mu = p_{1\mu} D_1 + p_{2\mu} D_2 + p_{3\mu} D_3 \quad (\text{B.4})$$

$$D_{\mu\nu} = g_{\mu\nu} D_{00} + p_{1\mu} p_{1\nu} D_{11} + p_{2\mu} p_{2\nu} D_{22} + p_{3\mu} p_{3\nu} D_{33} + (p_{1\mu} p_{2\nu} + p_{2\mu} p_{1\nu}) D_{12} + (p_{1\mu} p_{3\nu} + p_{3\mu} p_{1\nu}) D_{13} + (p_{3\mu} p_{2\nu} + p_{2\mu} p_{3\nu}) D_{23}. \quad (\text{B.5})$$

with the scalar 4-point functions $D_{i,ij}(p_1^2, p_{12}^2, p_{23}^2, p_3^2, p_2^2, p_{13}^2, m_0^2, m_1^2, m_2^2, m_3^2)$.

All the tensor coefficients can be algebraically reduced to the basic scalar integrals A_0 , B_0 , C_0 and D_0 . The analytical expression of all the scalar functions can be found in [31, 25].

Appendix C: One-loop amplitude

In this appendix, we use the fermion-vector boson coupling constants as defined in terms of the neutral-current and charged-current vertices

$$\begin{aligned} [f\bar{f}V_\mu] &= \gamma_\mu (g_V^{fL} \frac{1-\gamma_5}{2} + g_V^{fR} \frac{1+\gamma_5}{2}) \\ [u\bar{d}W_\mu^+] &= -\frac{1}{\sqrt{2}s_W} \gamma_\mu \left(\frac{1-\gamma_5}{2} \right) \end{aligned} \quad (\text{C.1})$$

in the following notation:

$$\begin{aligned} g_\gamma^{fL} &= g_\gamma^{fR} = -e_f \\ g_Z^{uL} &= -\frac{(1-2s_W^2 e_u)}{4s_W c_W}, \quad g_Z^{fR} = \frac{2s_W^2 e_f}{4s_W c_W} \\ g_Z^{dL} &= \frac{(1+2s_W^2 e_d)}{4s_W c_W} \\ e_u &= -2e_d = \frac{2}{3}|e|, \quad e_e = -|e|. \end{aligned} \quad (\text{C.2})$$

Vertex diagrams

Fermionic loops

d-d-u exchange

The diagram with the ddu triangle, Fig.1.1, yields the following contribution to the one-loop amplitude (3.2) for each V boson exchange ($V = \gamma, Z$):

$$\begin{aligned} M_{1.1} &= \frac{2N_C \alpha^2}{(\sqrt{2}(s-m_V^2)s_W)} \left(\{-(m_u Y_{ud}^L g_V^{dL} + m_d Y_{ud}^R (g_V^{dL} - g_V^{dR}))B_0(s, m_d^2, m_d^2) - \right. \\ &\quad m_u(m_u^2 Y_{ud}^L g_V^{dL} + m_d m_u Y_{ud}^R (g_V^{dL} - g_V^{dR}) - m_d^2 Y_{ud}^L g_V^{dR})C_0 + \\ &\quad 2(m_u Y_{ud}^L + m_d Y_{ud}^R)g_V^{dL}C_{00}\} [g_V^{eR} \mathcal{A}_1 + g_V^{eL} \mathcal{A}_2] \\ &\quad - \{(m_u (m_W^2 + u) Y_{ud}^L g_V^{dL} + m_d Y_{ud}^R (m_W^2 g_V^{dL} - t g_V^{dR}))C_1 + m_u u Y_{ud}^L g_V^{dL}C_0 \\ &\quad + (m_u (m_{H\pm}^2 + u) Y_{ud}^L g_V^{dL} + m_d Y_{ud}^R (u g_V^{dL} - m_{H\pm}^2 g_V^{dR}))C_2\} g_V^{eR} \mathcal{A}_1 + \\ &\quad \{[m_u (m_W^2 + t) Y_{ud}^L g_V^{dL} + m_d Y_{ud}^R (m_W^2 g_V^{dL} - u g_V^{dR})]C_1 - m_u t Y_{ud}^L g_V^{dL}C_0 + \\ &\quad [m_u (-m_{H\pm}^2 - t) Y_{ud}^L g_V^{dL} + m_d Y_{ud}^R (m_{H\pm}^2 g_V^{dR} - t g_V^{dL})]C_2\} g_V^{eL} \mathcal{A}_2 \\ &\quad - 2\{g_V^{dL} (m_u Y_{ud}^L C_0 + m_u Y_{ud}^L C_1 + (2m_u Y_{ud}^L + m_d Y_{ud}^R)C_2 + \\ &\quad (m_u Y_{ud}^L + m_d Y_{ud}^R)C_{12} + (m_u Y_{ud}^L + m_d Y_{ud}^R)C_{22})\} [g_V^{eR} \mathcal{A}_3 + g_V^{eL} \mathcal{A}_6] \end{aligned}$$

$$\begin{aligned}
& +2\{m_d Y_{ud}^R g_V^{dR} C_1 - g_V^{dL}(m_u Y_{ud}^L C_2 + \\
& (m_u Y_{ud}^L + m_d Y_{ud}^R)(C_{12} + C_{22}))\}[g_V^{eL} \mathcal{A}_4 + g_V^{eR} \mathcal{A}_5] \ .
\end{aligned} \tag{C.3}$$

Therein, all the C_i and C_{ij} have the same arguments: $(m_W^2, s, m_{H^\pm}^2, m_u^2, m_d^2, d_d^2)$. Summation has to be performed over all fermion families; in practice only the third quark generation is relevant.

u-u-d exchange

The corresponding expression for the the diagram with the uud triangle in Fig.1.2 is obtained from the previous one by making the following replacements:

$$Y_{ud}^L \longleftrightarrow Y_{ud}^R, \quad m_u \longleftrightarrow m_d, \quad g_V^{dL} \longleftrightarrow g_V^{uL}, \quad g_V^{dR} \longleftrightarrow g_V^{uR} \text{ and } t \longleftrightarrow u$$

and also $\mathcal{A}_3 \longleftrightarrow \mathcal{A}_5$ and $\mathcal{A}_6 \longleftrightarrow \mathcal{A}_4$.

Bosonic Loops

Listed are always the analytic expression for each generic diagram of Fig.1. The sum over all the particle contents, given in the associated tables, yields the corresponding contribution to the one-loop the matrix element (3.2).

Fig.1.3

$$\begin{aligned}
M_{1.3} = & -\frac{\alpha^2 g_{VW^+W^-}}{s - m_V^2} g_{W^+W^-} s g_{H^-W^+S} \{ \left(-B_0(s, m_W^2, m_W^2) - (m_S^2 - m_W^2 + s)C_0 + \right. \\
& (m_{H^\pm}^2 - m_W^2 - s)C_1 + (m_{H^\pm}^2 - m_W^2 + s)C_2 + C_{00} \left. \right) [g_V^{eR} \mathcal{A}_1 + g_V^{eL} \mathcal{A}_2] \\
& + (4C_1 + C_2 - C_{12} - C_{22})[g_V^{eR} (\mathcal{A}_3 + \mathcal{A}_5) + g_V^{eL} (\mathcal{A}_6 + \mathcal{A}_4)] \} .
\end{aligned} \tag{C.4}$$

All the C_i and C_{ij} have the same arguments: $(m_W^2, s, m_{H^\pm}^2, m_S^2, m_W^2, m_W^2)$. The couplings are summarized in the following table; S is a generic notation for one of the Higgs bosons.

S	g_{ZZS}	$g_{W^+W^-S}$	$g_{H^-W^+S}$	$g_{ZW^+W^-}$	$g_{\gamma W^+W^-}$
h	$m_Z \frac{s_{\beta\alpha}}{c_W s_W}$	$m_W \frac{s_{\beta\alpha}}{s_W}$	$\frac{c_{\beta\alpha}}{2s_W}$	$-\frac{c_w}{s_W}$	-1
H	$m_Z \frac{c_{\beta\alpha}}{c_W s_W}$	$m_W \frac{c_{\beta\alpha}}{s_W}$	$-\frac{s_{\beta\alpha}}{2s_W}$	$-\frac{c_w}{s_W}$	-1

Therein, $s_{\beta\alpha} \equiv \sin(\beta - \alpha)$ and $c_{\beta\alpha} \equiv \cos(\beta - \alpha)$.

Fig.1.4

$$\begin{aligned}
M_{1.4} = & \frac{2\alpha^2}{s - m_V^2} g_{VS_i S_j} g_{W^-W^+S_j} g_{H^-W^+S_i} \{ C_{00} [g_V^{eR} \mathcal{A}_1 + g_V^{eL} \mathcal{A}_2] \\
& - (2C_0 + 2C_1 + 3C_2 + C_{12} + C_{22})[g_V^{eR} (\mathcal{A}_3 + \mathcal{A}_5) + g_V^{eL} (\mathcal{A}_6 + \mathcal{A}_4)] \} \tag{C.5}
\end{aligned}$$

where the arguments of C_i and C_{ij} are now as follows: $(m_W^2, s, m_{H^\pm}^2, m_W^2, m_{S_i}^2, m_{S_j}^2)$. The couplings are summarized in the following table:

(S_i, S_j)	$g_{ZS_iS_j}$	$g_{H^-S_iW}$	$g_{W^-W^+S_j}$
(A_0, h)	$\frac{c_{\beta\alpha}}{2s_W c_W}$	$\frac{1}{2s_W}$	$s_{\beta\alpha} \frac{m_W}{s_W}$
(A_0, H)	$-\frac{s_{\beta\alpha}}{2s_W c_W}$	$\frac{1}{2s_W}$	$c_{\beta\alpha} \frac{m_W}{s_W}$

Fig.1.5

$$\begin{aligned}
M_{1.5} = & \frac{\alpha^2}{s - m_V^2} g_{VS_iS_j} g_{W^+S_jS_k} g_{H^-S_iS_k} \{C_{00}[g_V^{eR} \mathcal{A}_1 + g_V^{eL} \mathcal{A}_2] - \\
& (C_2 + C_{12} + C_{22})[g_V^{eR} (\mathcal{A}_3 + \mathcal{A}_5) + g_V^{eL} (\mathcal{A}_6 + \mathcal{A}_4)]\} \tag{C.6}
\end{aligned}$$

All the C_i and C_{ij} have the same arguments: $(m_W^2, s, m_{H^\pm}^2, m_{S_k}^2, m_{S_i}^2, m_{S_j}^2)$. The couplings are summarized in the following table:

(S_i, S_j, S_k)	$g_{\gamma S_i S_j}$	$g_{ZS_iS_j}$	$g_{H^\pm S_i S_k}$	$g_{W^+ S_j S_k}$
(A_0, h, G^\pm)	0	$i \frac{c_{\beta\alpha}}{2s_W c_W}$	$ig_{H^-A_0G^+}$	$\frac{s_{\beta\alpha}}{2s_W}$
(A_0, H, G^\pm)	0	$-i \frac{s_{\beta\alpha}}{2s_W c_W}$	$ig_{H^+A_0G^-}$	$\frac{c_{\beta\alpha}}{2s_W}$
(G^\pm, G^\pm, h)	-1	$-\frac{\cos(2\theta_W)}{2s_W c_W}$	$g_{H^-hG^+}$	$\frac{s_{\beta\alpha}}{2s_W}$
(G^\pm, G^\pm, H)	-1	$-\frac{\cos(2\theta_W)}{2s_W c_W}$	$g_{H^-HG^+}$	$\frac{c_{\beta\alpha}}{2s_W}$
(H^\pm, H^\pm, h)	-1	$-\frac{\cos(2\theta_W)}{2s_W c_W}$	$g_{H^-hH^+}$	$\frac{c_{\beta\alpha}}{2s_W}$
(H^\pm, H^\pm, H)	-1	$-\frac{\cos(2\theta_W)}{2s_W c_W}$	$g_{H^-HH^+}$	$-\frac{s_{\beta\alpha}}{2s_W}$

where the $g_{H^\pm S_i S_k}$ couplings have been defined in appendix A.

Fig.1.6

$$M_{1.6} = -\frac{\alpha^2}{s - m_V^2} g_{VV'S_i} g_{W^+V'S_j} g_{H^-S_iS_j} C_0 [g_V^{eR} \mathcal{A}_1 + g_V^{eL} \mathcal{A}_2] \tag{C.7}$$

where $C_0 = C_0(m_W^2, s, m_{H^\pm}^2, m_{S_i}^2, m_{S_j}^2, m_{V'}^2)$. The couplings are summarized in the following table:

(S_i, S_j, V')	$g_{\gamma V' S_i}$	$g_{ZV' S_i}$	$g_{H^+ S_i S_j}$	$g_{W^+ V' S_j}$
(h, G^\pm, Z)	0	$m_Z \frac{s_{\beta\alpha}}{s_W c_W}$	$g_{H^-G^+h}$	$-m_Z s_W$
(H, G^\pm, Z)	0	$m_Z \frac{c_{\beta\alpha}}{s_W c_W}$	$g_{H^-G^+H}$	$-m_Z s_W$
(G^\pm, h, W^\pm)	m_W	$-m_Z s_W$	$g_{H^-G^+h}$	$s_{\beta\alpha} \frac{m_W}{s_W}$
(G^\pm, H, W^\pm)	m_W	$-m_Z s_W$	$g_{H^-G^+H}$	$c_{\beta\alpha} \frac{m_W}{s_W}$

Fig.1.7

$$\begin{aligned}
M_{1.7} = & \frac{2\alpha^2}{s - m_V^2} g_{VV'S_i} g_{W^+S_iS_j} g_{H^-V'S_j} \{ -C_{00} [g_V^{eR} \mathcal{A}_1 + g_V^{eL} \mathcal{A}_2] + \\
& (-C_2 + C_{12} + C_{22}) [g_V^{eR} (\mathcal{A}_3 + \mathcal{A}_5) + g_V^{eL} (\mathcal{A}_6 + \mathcal{A}_4)] \}
\end{aligned} \quad (C.8)$$

All the C_i and C_{ij} have the same arguments: $(m_W^2, s, m_{H^\pm}^2, m_{S_i}^2, m_{S_j}^2, m_{V'}^2)$. The couplings are summarized in the following table:

(S_i, S_j)	$g_{\gamma W^+ S_i}$	$g_{ZW^+ S_i}$	$g_{H^- W^+ S_j}$	$g_{W^+ S_i S_j}$
(G^\pm, h)	m_w	$-m_Z s_W$	$\frac{c_{\beta\alpha}}{2s_W}$	$\frac{s_{\beta\alpha}}{2s_W}$
(G^\pm, H)	m_W	$-m_Z s_W$	$-\frac{s_{\beta\alpha}}{2s_W}$	$\frac{c_{\beta\alpha}}{2s_W}$

Fig.1.8

$$\begin{aligned}
M_{1.8} = & -\frac{\alpha^2}{s - m_Z^2} g_{ZZS} g_{ZW^-W^+} g_{H^-W^+S} \{ (B_0(s, m_S^2, m_Z^2) + (2m_{H^\pm}^2 + 3m_W^2 - 2s)C_0 \\
& + [m_{H^\pm}^2 + 3m_W^2 - s]C_1 + [3m_{H^\pm}^2 + m_W^2 - s]C_2 - C_{00}) [g_V^{eR} \mathcal{A}_1 + g_V^{eL} \mathcal{A}_2] \\
& (2C_0 - 2C_1 + 3C_2 + C_{12} + C_{22}) [g_V^{eR} (\mathcal{A}_3 + \mathcal{A}_5) + g_V^{eL} (\mathcal{A}_6 + \mathcal{A}_4)] \}
\end{aligned} \quad (C.9)$$

where all the C_i and C_{ij} have the same arguments: $(m_W^2, s, m_{H^\pm}^2, m_W^2, m_Z^2, m_S^2)$. The couplings are summarized in the following table:

S	g_{ZZS}	$g_{H^-W^+S}$	$g_{ZW^-W^+}$
h	$m_Z \frac{s_{\beta\alpha}}{s_W c_W}$	$\frac{c_{\beta\alpha}}{2s_W}$	$-\frac{c_w}{s_W}$
H	$m_Z \frac{c_{\beta\alpha}}{s_W c_W}$	$-\frac{s_{\beta\alpha}}{2s_W}$	$-\frac{c_w}{s_W}$

Fig.1.9

$$M_{1.9} = \frac{\alpha^2}{s - m_V^2} g_{VW^+H^-S_1} g_{W^+W^-S_1} \{ B_0(m_W^2, m_{S_1}^2, m_W^2) [g_V^{eR} \mathcal{A}_1 + g_V^{eL} \mathcal{A}_2] \} \quad (C.10)$$

Fig.1.10

$$M_{1.10} = -\frac{\alpha^2}{s - m_V^2} g_{VW^+S_1S_2} g_{H^-S_1S_2} \{ B_0(m_{H^\pm}^2, m_S^2, m_{H^\pm}^2) [g_V^{eR} \mathcal{A}_1 + g_V^{eL} \mathcal{A}_2] \} \quad (C.11)$$

Fig.1.11

$$M_{1.11} = \frac{\alpha^2}{s - m_Z^2} g_{ZW^+H^-S_1} g_{SZZ} \{ B_0(s, m_{S_1}^2, m_Z^2) [g_V^{eR} \mathcal{A}_1 + g_V^{eL} \mathcal{A}_2] \} \quad (\text{C.12})$$

where the couplings are given in the table

(S_1, S_2)	$g_{ZW^+S_1S_2}$	$g_{\gamma W^+S_1S_2}$	$g_{H^-S_1S_2}$
(h, H^-)	$-\frac{c_{\beta\alpha}}{2c_W}$	$\frac{c_{\beta\alpha}}{2s_W}$	$g_{hH^-H^-}$
(H, H^-)	$\frac{s_{\beta\alpha}}{2c_W}$	$-\frac{s_{\beta\alpha}}{2s_W}$	$g_{HH^-H^-}$
(h, G^+)	$-\frac{s_{\beta\alpha}}{2c_W}$	$\frac{s_{\beta\alpha}}{2s_W}$	$g_{hH^-G^+}$
(H, G^+)	$-\frac{c_{\beta\alpha}}{2c_W}$	$\frac{s_{\beta\alpha}}{2s_W}$	$g_{HH^-G^+}$

Box diagrams

Fig.1.12

$$M_h^{Box} = -\frac{\alpha^2}{4s_W^2} c_{\beta\alpha} s_{\beta\alpha} m_W \{ [C_0(m_e^2, m_e^2, s, m_W^2, 0, m_W^2) + (m_h^2 - u)D_0 + (m_W^2 - u)D_1 + (m_W^2 - s - t)D_3] \mathcal{A}_2 - 4D_1 \mathcal{A}_4 \} \quad (\text{C.13})$$

where all the D_i functions have as arguments: $(m_W^2, m_e^2, m_e^2, m_{H^\pm}^2, s, m_h^2, m_W^2, 0, m_W^2)$. The corresponding box graph with a heavy neutral scalar is obtained by the substitution

$$M_H^{Box} = -M_h^{Box}(m_h \rightarrow m_H) \quad (\text{C.14})$$

Counter-term diagrams

Denoting by $k^\mu \Sigma_{HW}(k^2)$ the bare $H^\pm W^\pm$ 2-point function, Fig.1.17 - Fig.1.20, the renormalized one is obtained by adding the counter-term (4.2). The renormalized non-diagonal self-energy $\hat{\Sigma}_{HW}(k^2)$ is thus given by:

$$\hat{\Sigma}_{HW}(k^2) = \Sigma_{HW}(k^2) - \Delta. \quad (\text{C.15})$$

According to the condition (4.6), requiring that the renormalized $W^+ - H^-$ mixing vanishes, Δ is determined by:

$$\Delta = \text{Re } \Sigma_{HW}(m_{H^\pm}^2). \quad (\text{C.16})$$

The self-energy $\Sigma_{HW}(m_{H^\pm}^2) \equiv \Sigma_{HW}$ has the following explicit form:

$$\Sigma_{HW} = \Sigma_{HW}^{ferm} + \Sigma_{HW}^{bos}.$$

The fermionic part is the sum over the individual fermion families, each one contributing

$$\Sigma_{HW}^{ud} = -N_C \frac{\alpha}{2\sqrt{2}s_W\pi} (m_d Y_{ud}^R B_0(m_{H^+}^2, m_d^2, m_u^2) + (m_u Y_{ud}^L + m_d Y_{ud}^R) B_1(m_{H^+}^2, m_d^2, m_u^2)), \quad (\text{C.17})$$

and the bosonic part is given by

$$\begin{aligned} \Sigma_{HW}^{bos} = & \frac{\alpha}{8\pi s_W^2} (c_{\beta\alpha} g_{hH^-H^-} s_W B_0(m_{H^\pm}^2, m_h^2, m_{H^\pm}^2) - c_{\beta\alpha} m_W s_{\beta\alpha} B_0(m_{H^\pm}^2, m_h^2, m_W^2) + \\ & g_{hH^-G^+} s_{\beta\alpha} s_W B_0(m_{H^\pm}^2, m_h^2, m_W^2) - g_{HH^+H^-} s_{\beta\alpha} s_W B_0(m_{H^\pm}^2, m_h^2, m_{H^\pm}^2) + \\ & c_{\beta\alpha} m_W s_{\beta\alpha} B_0(m_{H^\pm}^2, m_h^2, m_W^2) + c_{\beta\alpha} g_{HH^-G^+} s_W B_0(m_{H^\pm}^2, m_h^2, m_W^2) + \\ & 2c_{\beta\alpha} g_{hH^+H^-} s_W B_1(m_{H^\pm}^2, m_h^2, m_{H^\pm}^2) + c_{\beta\alpha} m_W s_{\beta\alpha} B_1(m_{H^\pm}^2, m_h^2, m_W^2) + \\ & 2g_{hH^+G^+} s_{\beta\alpha} s_W B_1(m_{H^\pm}^2, m_h^2, m_W^2) - 2g_{HH^+H^-} s_{\beta\alpha} s_W B_1(m_{H^\pm}^2, m_h^2, m_{H^\pm}^2) - \\ & c_{\beta\alpha} m_W s_{\beta\alpha} B_1(m_{H^\pm}^2, m_h^2, m_W^2) + 2c_{\beta\alpha} g_{HH^+G^+} s_W B_1(m_{H^\pm}^2, m_h^2, m_W^2)). \end{aligned} \quad (\text{C.18})$$

Then the amplitudes containing the counter terms, Fig.1.28, read:

$$M_{\delta(VWH)} = \frac{4\pi\alpha g_V}{s - m_V^2} \text{Re}(\Sigma_{HW}) [g_V^{eR} \mathcal{A}_1 + g_V^{eL} \mathcal{A}_2] \quad (\text{C.19})$$

with $g_Z = -s_W/c_W$, $g_\gamma = -1$ and $g_V^{eL,R}$ defined in (C.1)

Amplitudes with non-diagonal self-energies

t-channel W^+H^- mixing

The generic diagram for this topology is depicted in Fig.1.13. The amplitude contains only the invariant \mathcal{A}_2 :

$$M_{1.13} = \frac{e^2}{2s_W^2} \frac{\text{Im}(\Sigma_{HW}^{ferm}) + \text{Im}(\Sigma_{HW}^{bos})}{m_{H^\pm}^2 - m_W^2} \mathcal{A}_2 \quad (\text{C.20})$$

s-channel W^+H^- mixing

The generic diagram for this topology is depicted in Fig.1.15. The amplitude can be projected on $\mathcal{A}_{1,2}$ as follows:

$$M_{1.15} = \frac{e^2 g_{VWW}}{(s - m_V^2)} (m_W^2 - s) \frac{\text{Im}(\Sigma_{HW}^{ferm}) + \text{Im}(\Sigma_{HW}^{bos})}{m_{H^\pm}^2 - m_W^2} (g_V^{eR} \mathcal{A}_1 + g_V^{eL} \mathcal{A}_2) \quad (\text{C.21})$$

where $g_{ZWW} = c_W/s_W$ and $g_{\gamma WW} = 1$

s-channel $G^+ - H^-$ mixing

The non-diagonal Goldstone- H^\pm self-energy is Σ_{GH} evaluated in the same way as done before for the W - H^\pm case ($k^2 = m_{H^\pm}^2$):

$$\Sigma_{GH} = \Sigma_{GH}^{ferm} + \Sigma_{GH}^{bos},$$

where the fermionic part is obtained by summing over the families with

$$\begin{aligned} \Sigma_{GH}^{ud} = & \frac{-\alpha N_C}{(2\sqrt{2}m_W\pi s_W)} \{ (m_u Y_{ud}^L - m_d Y_{ud}^R) A_0(m_d^2) + m_u(-m_d^2 + m_u^2) Y_{ud}^L B_0(m_{H^\pm}^2, m_d^2, m_u^2) \\ & + m_{H^\pm}^2 (m_u Y_{ud}^L - m_d Y_{ud}^R) B_1(m_{H^\pm}^2, m_u^2, m_d^2) \}, \end{aligned} \quad (\text{C.22})$$

and the bosonic part is given by

$$\begin{aligned} \Sigma_{GH}^{bos} = & \frac{\alpha}{4\pi} \{ g_{hH^+H^-} g_{hG^+H^-} B_0(m_{H^\pm}^2, m_h^2, m_{H^\pm}^2) + g_{HH^+H^-} g_{HG^+H^-} B_0(m_{H^\pm}^2, m_H^2, m_{H^\pm}^2) \\ & + g_{hG^+H^-} g_{hG^+G^-} B_0(m_{H^\pm}^2, m_h^2, m_W^2) + g_{HG^+H^-} g_{HG^+G^-} B_0(m_{H^\pm}^2, m_H^2, m_W^2) - \\ & \frac{s_{\beta\alpha}c_{\beta\alpha}}{4s_W^2} (A_0(m_W^2) + (m_h^2 + m_{H^\pm}^2) B_0(m_{H^\pm}^2, m_h^2, m_W^2) - 2m_{H^\pm}^2 B_1(m_{H^\pm}^2, m_h^2, m_W^2) + \\ & - (A_0(m_W^2) + (m_H^2 + m_{H^\pm}^2) B_0(m_{H^\pm}^2, m_H^2, m_W^2) - 2m_{H^\pm}^2 B_1(m_{H^\pm}^2, m_H^2, m_W^2))) \}. \end{aligned} \quad (\text{C.23})$$

Then the amplitude of the diagram Fig.1.14 can be written in the form

$$M_{1.14} = \frac{e^2 g_{VW^+G^-}}{(s - m_V^2)} \frac{\text{Im}(\Sigma_{GH}^{ud}) + \text{Im}(\Sigma_{GH}^{bos})}{m_{H^\pm}^2 - m_W^2} (g_V^{eR} \mathcal{A}_1 + g_V^{eL} \mathcal{A}_2) \quad (\text{C.24})$$

where $g_{ZW^+G^-} = -m_W s_W / c_W$ and $g_{\gamma W^+G^-} = m_W$.

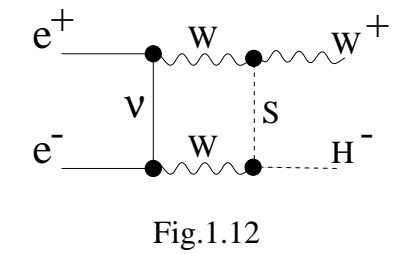
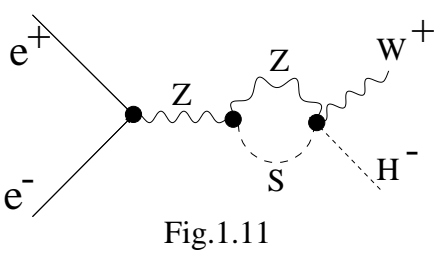
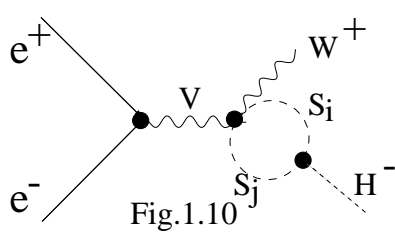
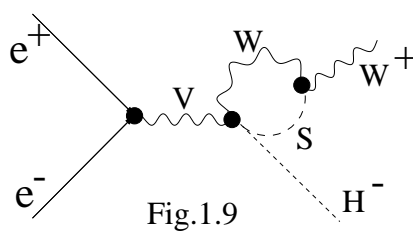
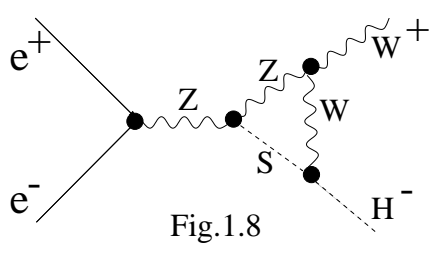
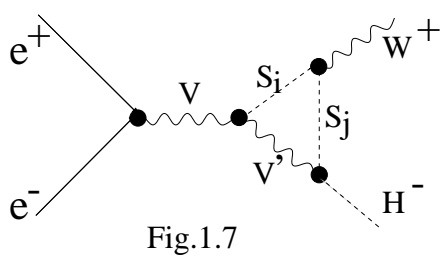
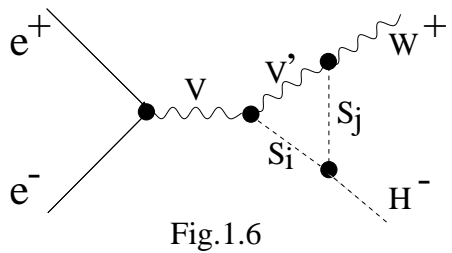
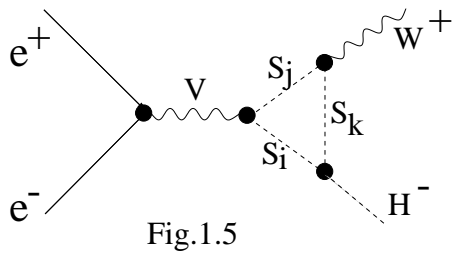
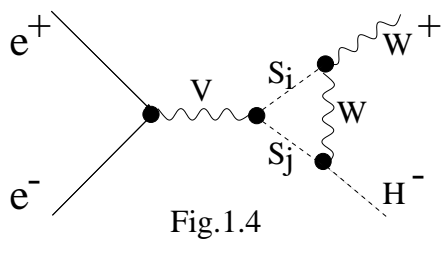
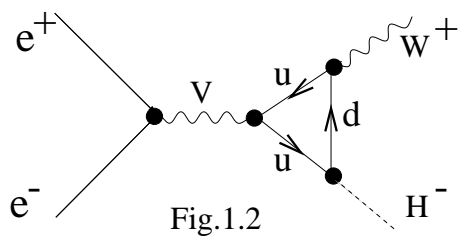
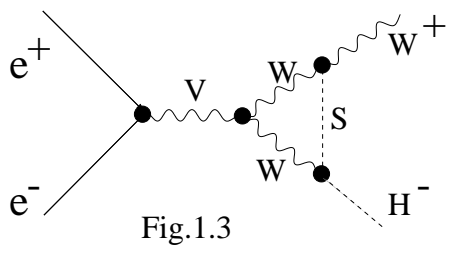
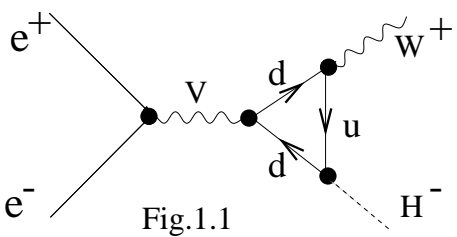


Figure. 1

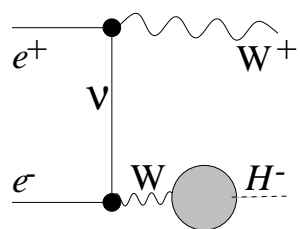


Fig.1.13

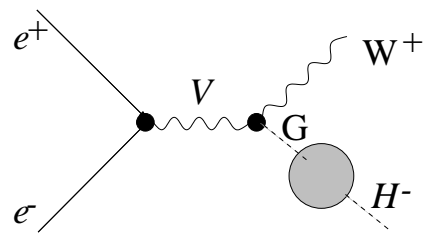


Fig.1.14

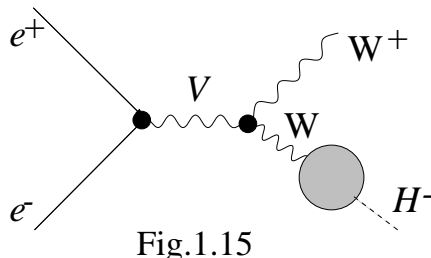


Fig.1.15

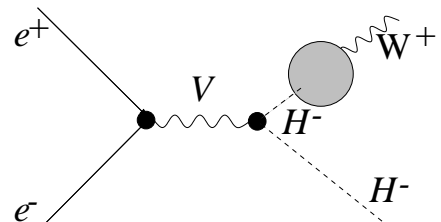


Fig.1.16

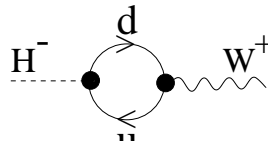


Fig.1.17

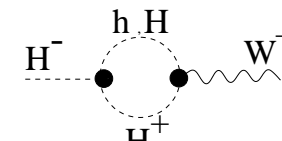


Fig.1.18

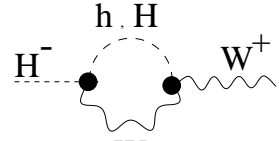


Fig.1.19

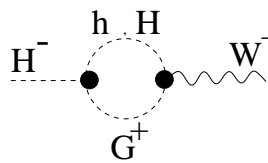


Fig.1.20

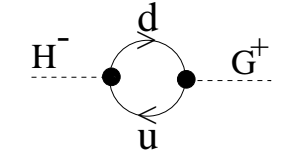


Fig.1.21

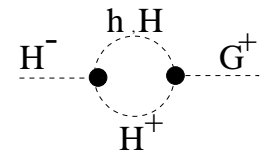


Fig.1.22

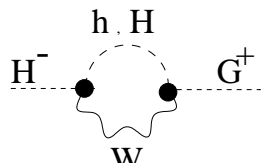


Fig.1.23

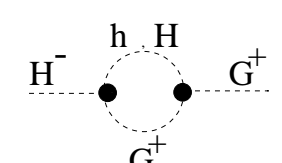


Fig.1.24

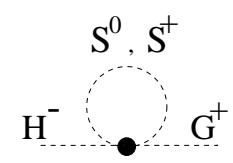


Fig.1.25

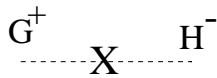


Fig.1.26

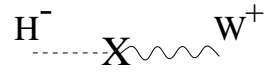


Fig.1.27

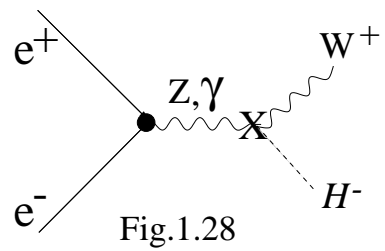


Fig.1.28

Figure.1 (cont.)

Fig 2. a

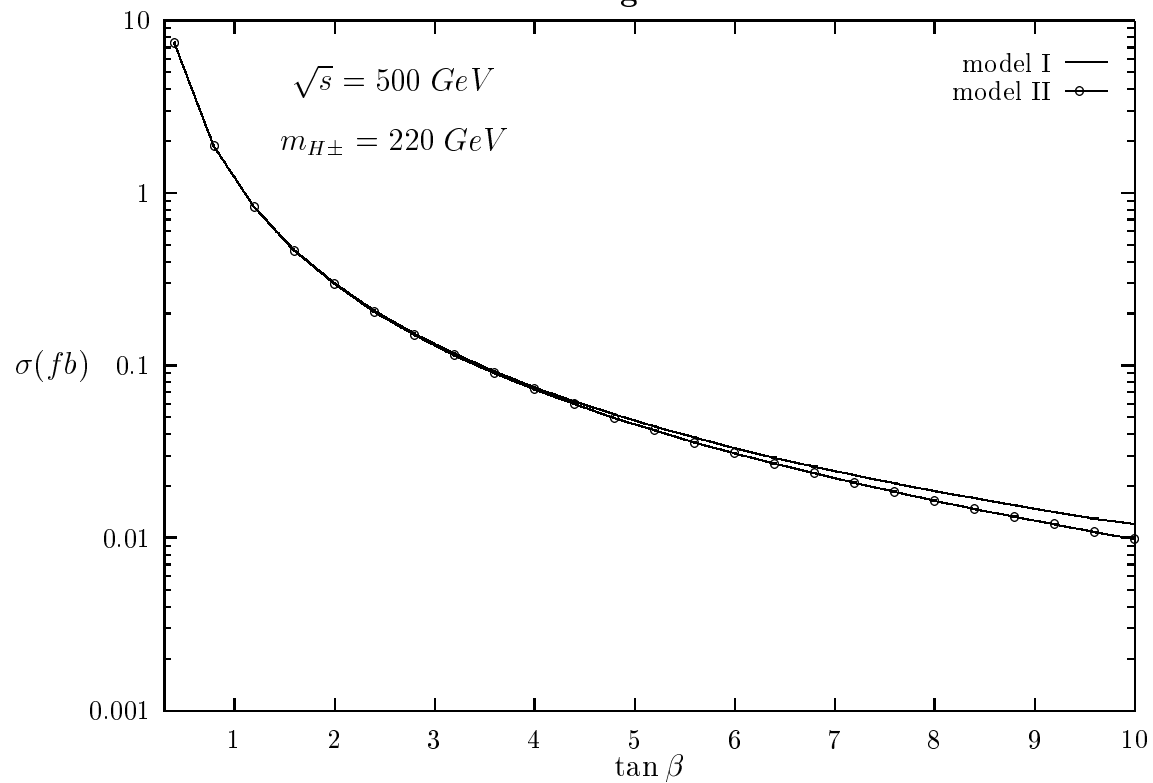


Fig 2. b

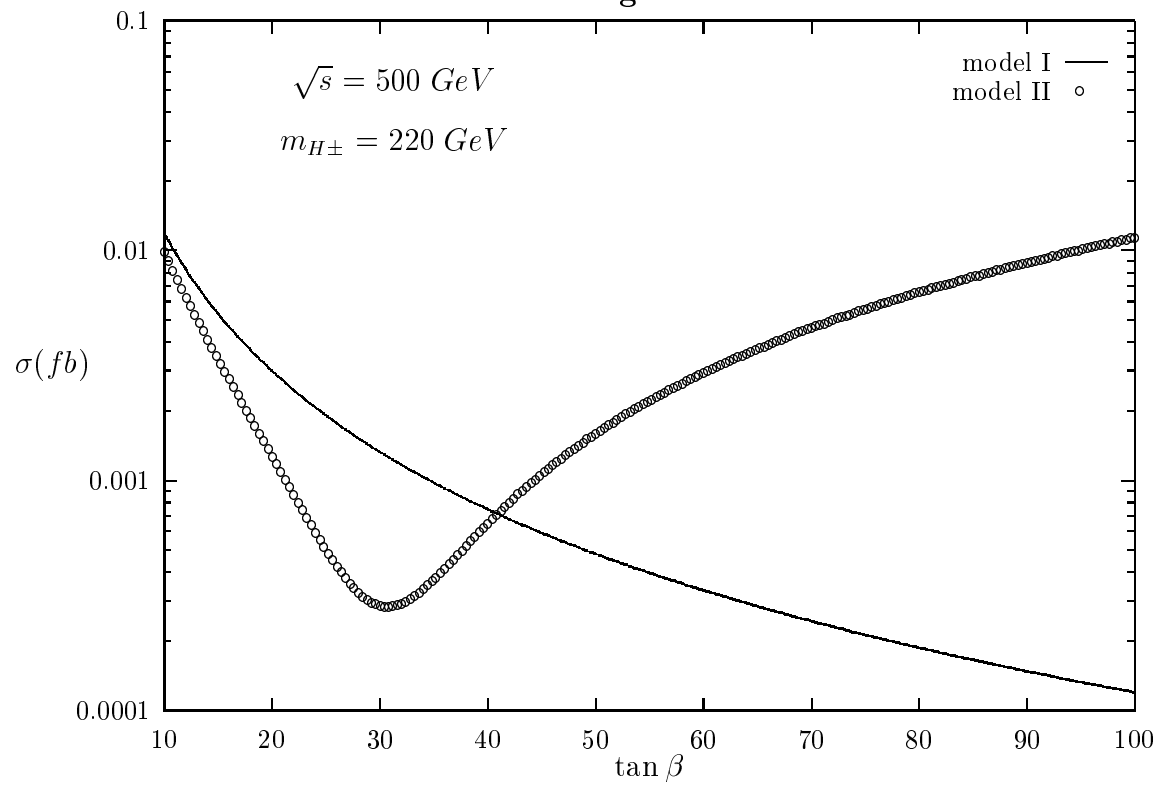


Figure. 2

Fig 3. a

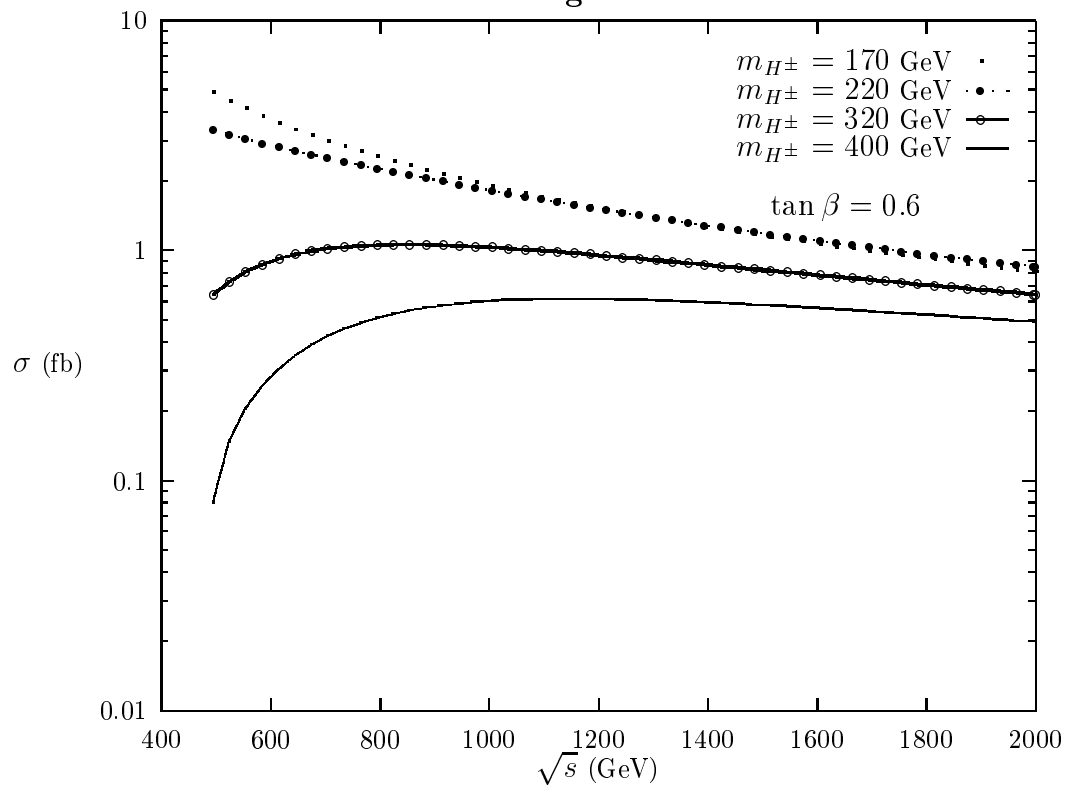


Fig 3. b

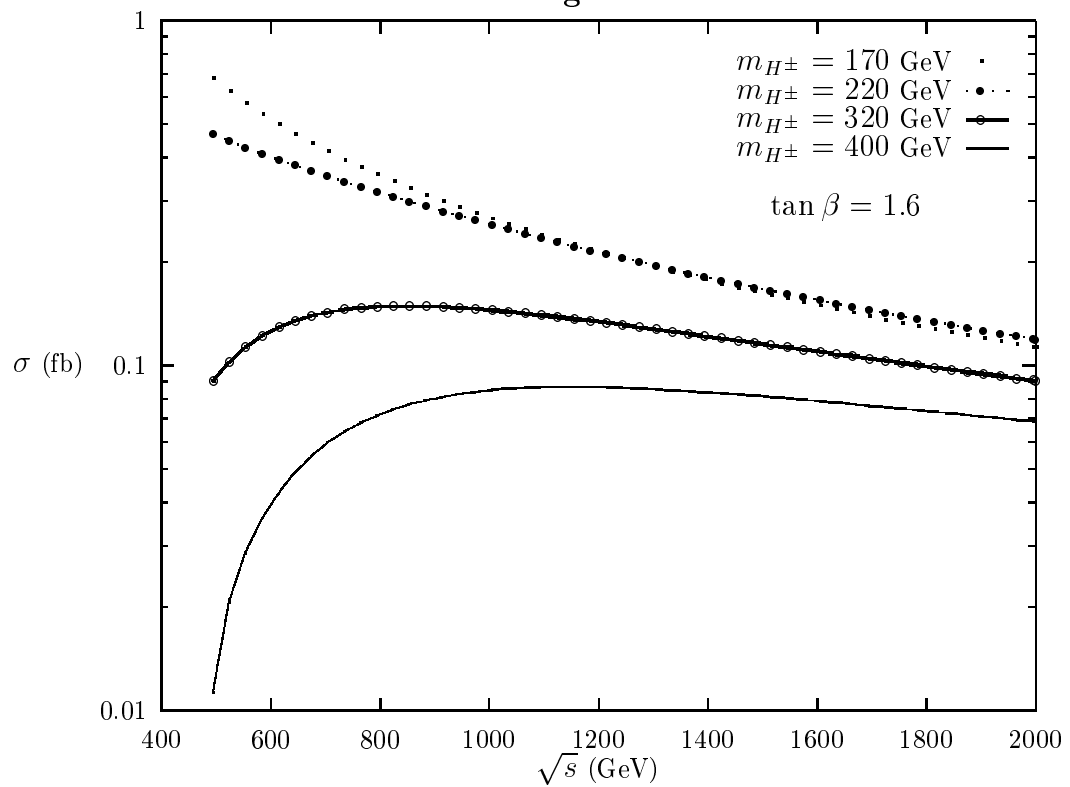


Figure. 3

Fig 4. a (C_1 case)

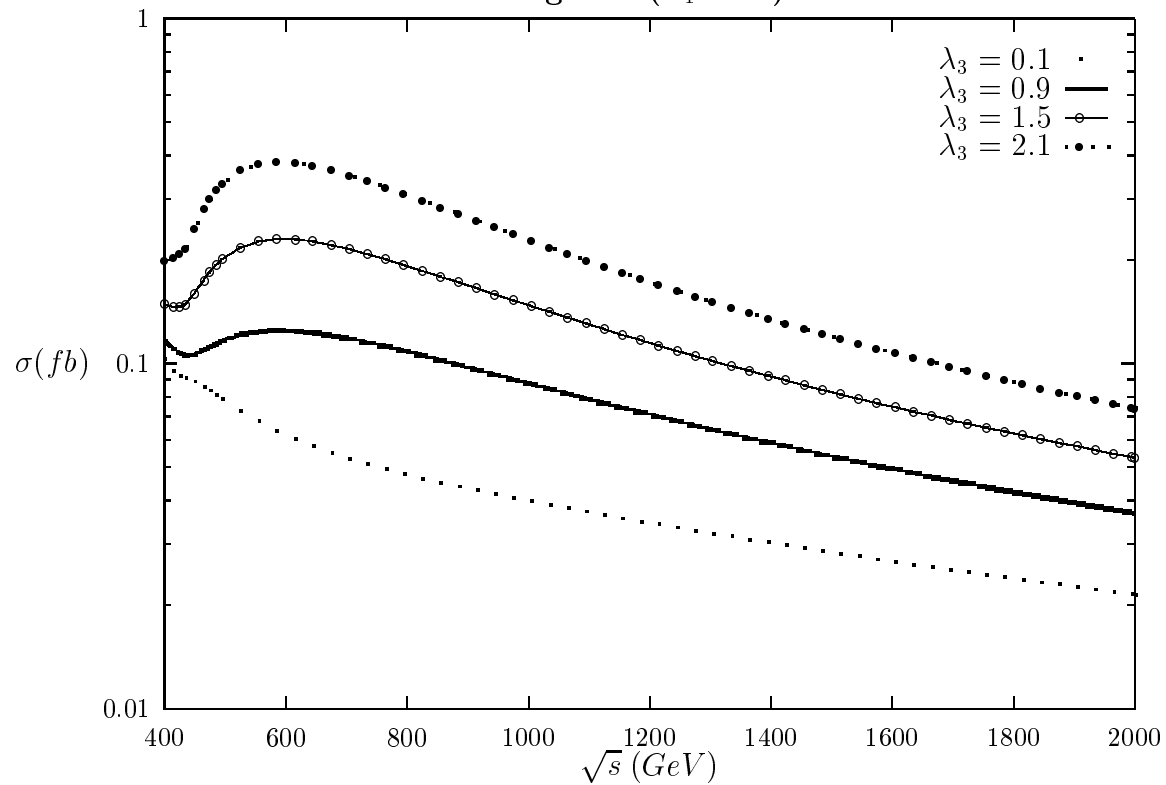


Fig 4. b (C_2 case)

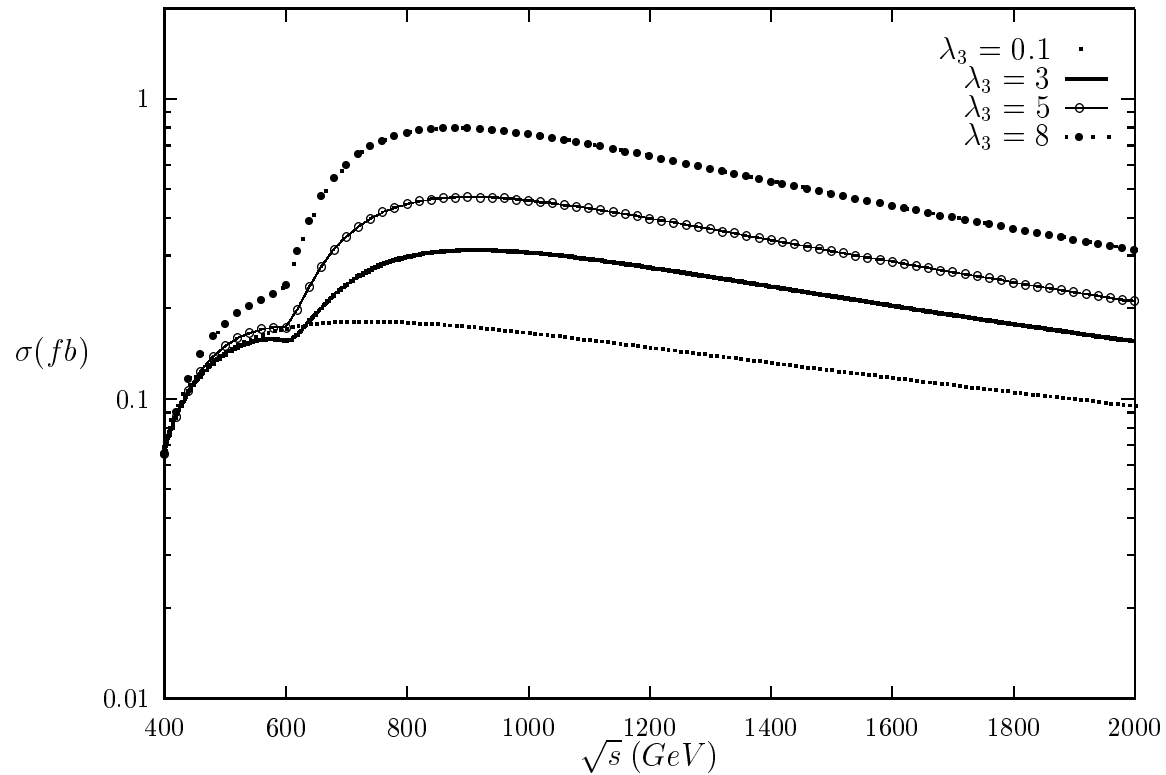


Figure. 4

Fig 4. c (C_3 case)

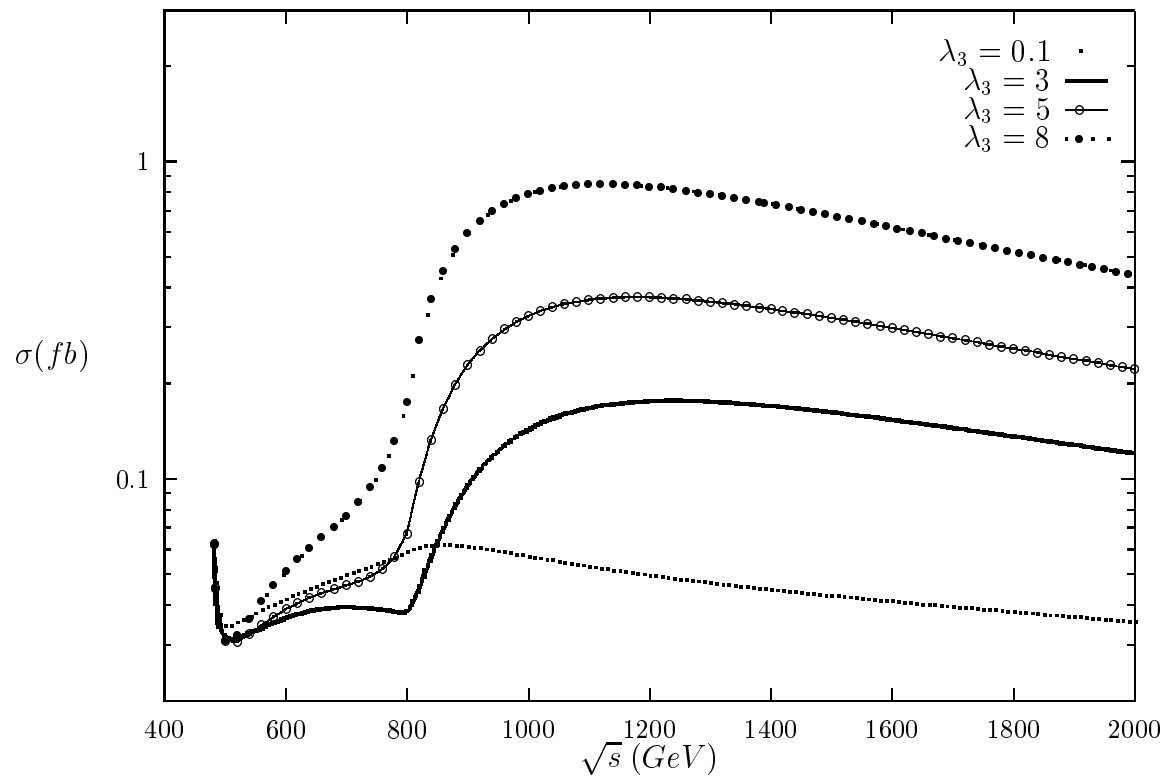


Fig 4. d (Boxes)

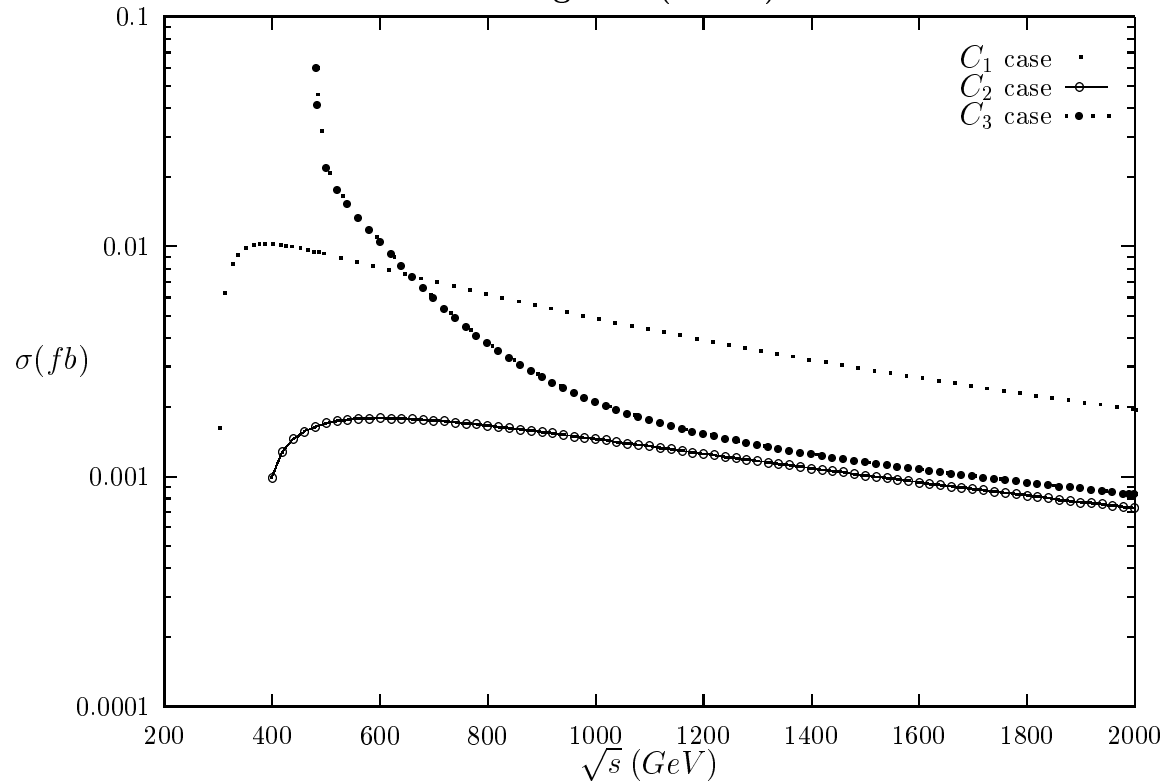


Figure. 4 (cont.)

Fig 5. a

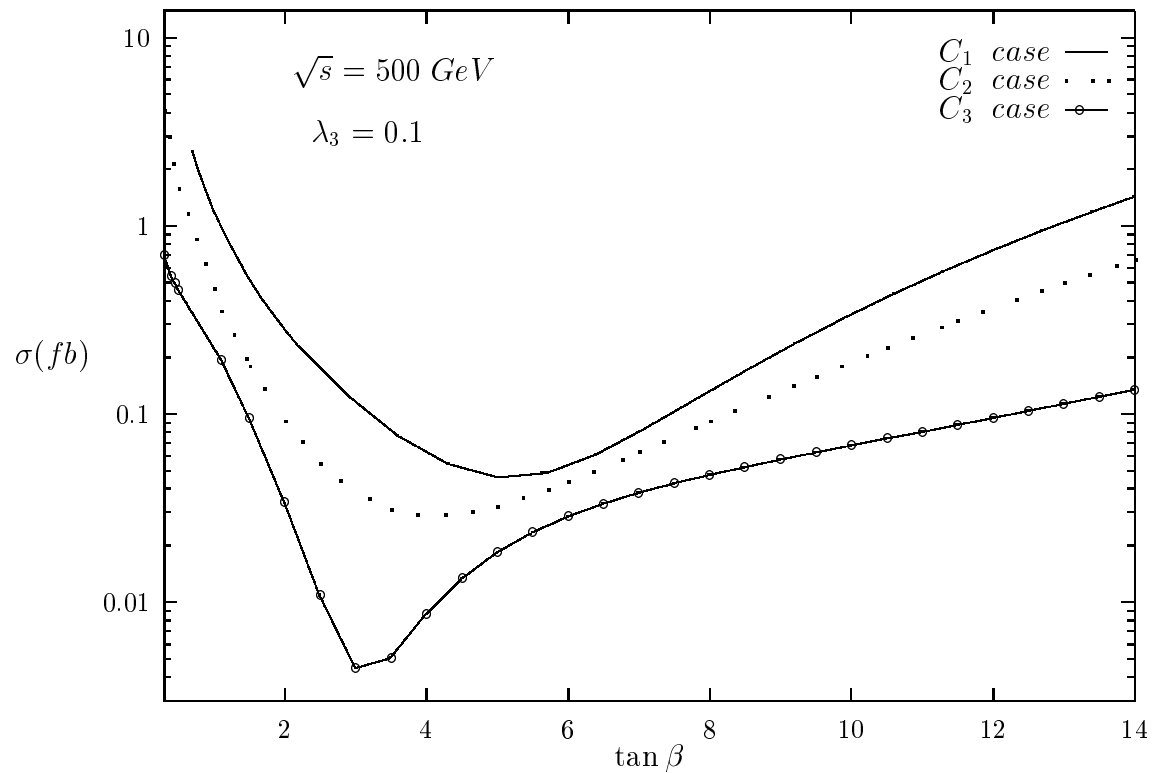


Fig 5. b

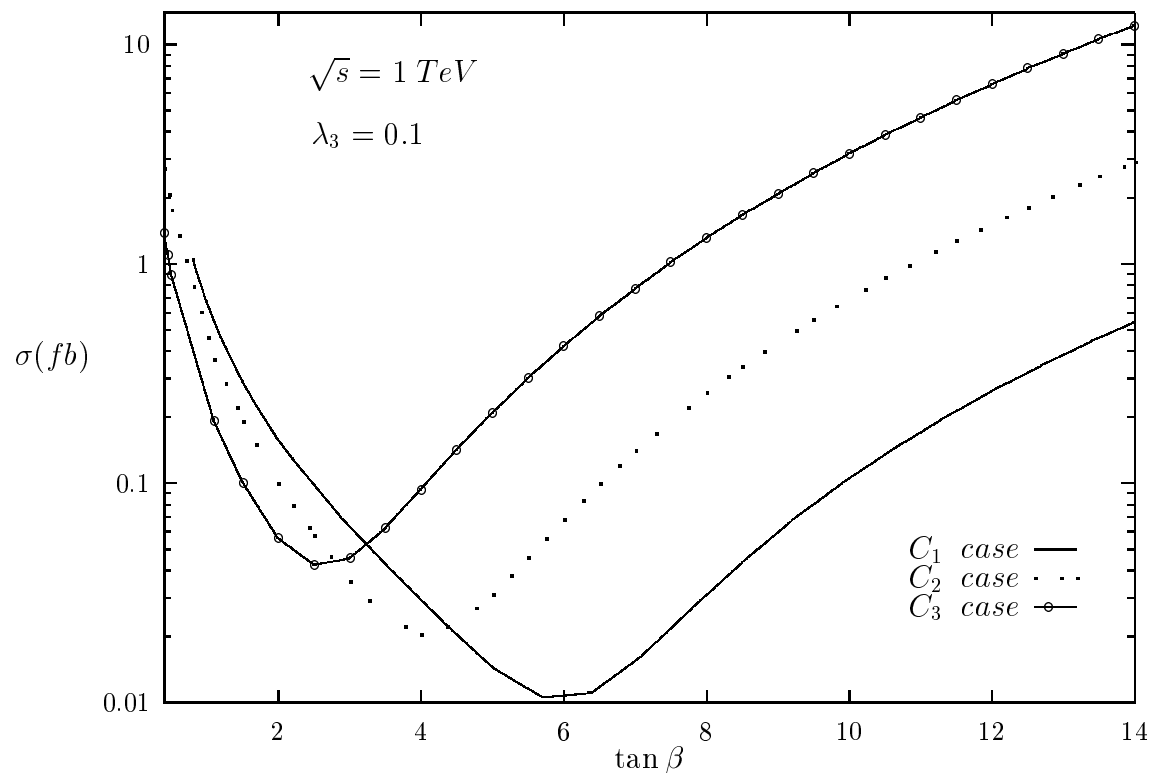


Figure. 5

Fig 5. c

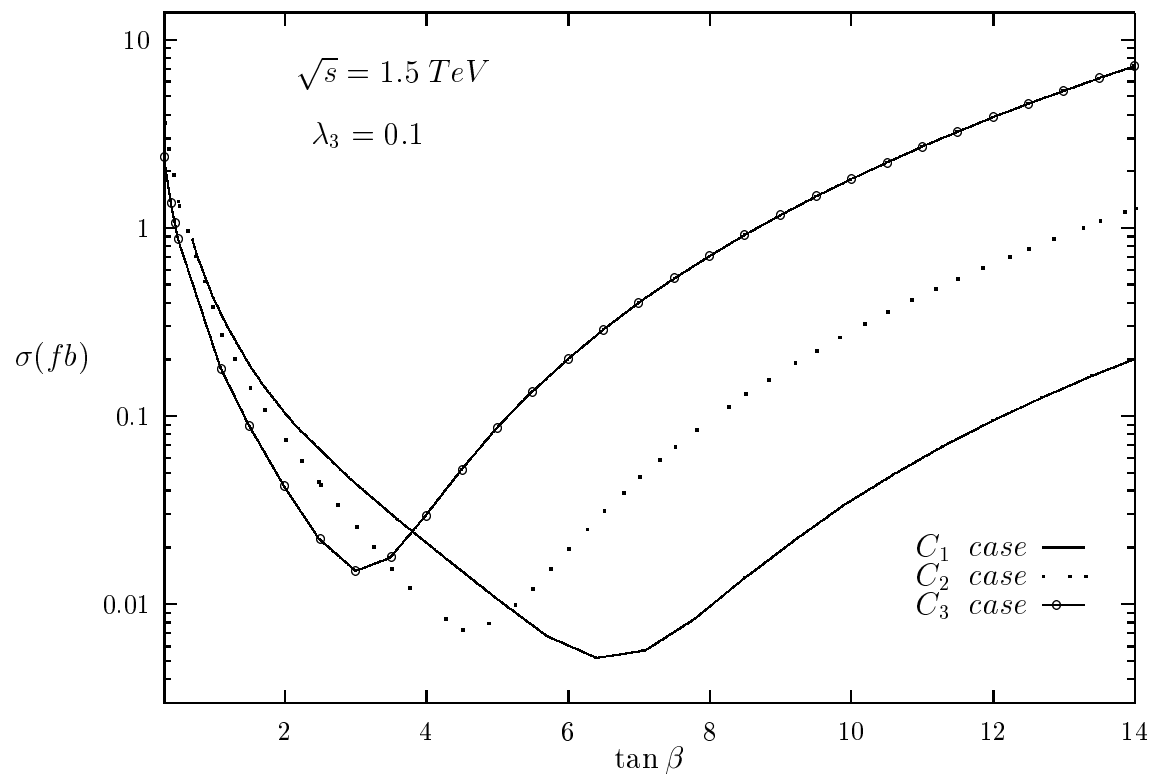


Figure. 5 (cont.)

Fig 6.

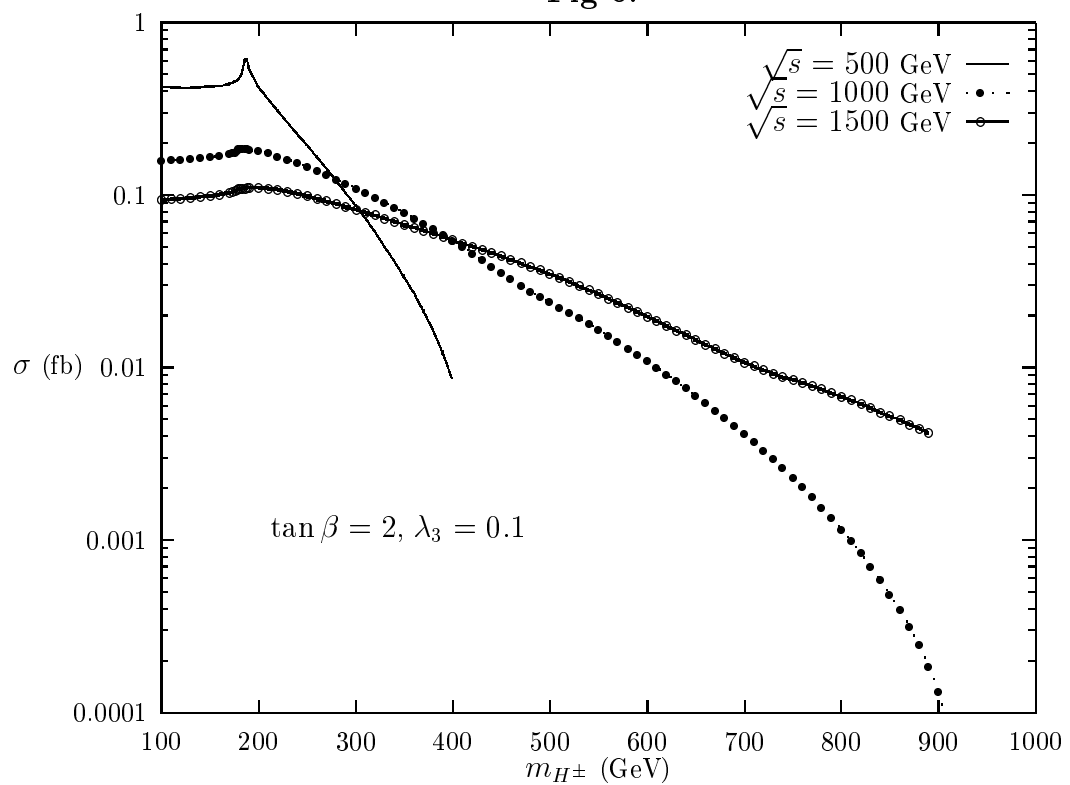


Figure. 6